

Competing structures in two dimensions: square-to-hexagonal transition

Barbara Gränz,¹ Sergey E. Korshunov,² Vadim B. Geshkenbein,¹ and Gianni Blatter¹

¹*Theoretische Physik, ETH Zurich, CH-8093 Zurich, Switzerland*

²*L.D. Landau Institute for Theoretical Physics, 142432 Chernogolovka, Russia*

(Dated: August 25, 2021)

We study a system of particles in two dimensions interacting via a dipolar long-range potential D/r^3 and subject to a square-lattice substrate potential $V(\mathbf{r})$ with amplitude V and lattice constant b . The isotropic interaction favors a hexagonal arrangement of the particles with lattice constant a , which competes against the square symmetry of the underlying substrate lattice. We determine the minimal-energy states at fixed external pressure p generating the commensurate density $n = 1/b^2 = (4/3)^{1/2}/a^2$ in the absence of thermal and quantum fluctuations, using both analytical techniques based on the harmonic- and continuum elastic approximations as well as numerical relaxation of particle configurations. At large substrate amplitude $V > 0.2e_D$, with $e_D = D/b^3$ the dipolar energy scale, the particles reside in the substrate minima and hence arrange in a square lattice. Upon decreasing V , the square lattice turns unstable with respect to a zone-boundary shear-mode and deforms into a period-doubled zig-zag lattice. Analytic and numerical results show that this period-doubled phase in turn becomes unstable at $V \approx 0.074e_D$ towards a non-uniform phase developing an array of domain walls or solitons; as the density of solitons increases, the particle arrangement approaches that of a rhombic (or isosceles triangular) lattice. At a yet smaller substrate value estimated as $V \approx 0.046e_D$, a further solitonic transition establishes a second non-uniform phase which smoothly approaches the hexagonal (or equilateral triangular) lattice phase with vanishing amplitude V . At small but finite amplitude V , the hexagonal phase is distorted and hexatically locked at an angle of $\varphi \approx 3.8^\circ$ with respect to the substrate lattice. The square-to-hexagonal transformation in this two-dimensional commensurate-incommensurate system thus involves a complex pathway with various non-trivial lattice- and modulated phases.

I. INTRODUCTION

Interacting particles exhibit complex structural changes when subjected to an external modulated potential. A periodic modulation which is out of registry with the particle lattice can induce lattice distortions, favor alternative lattices, or generate non-uniform phases in commensurate-incommensurate transitions¹, where solitons separate different regions of locked phases. On the other hand, a random potential typically leads to the loss of long-range order². Besides such structural changes, both, periodic and random potentials lead to pinning of the particles to the substrate, thereby changing their dynamics under the action of an applied force, a phenomenon which is of particular importance in the context of dissipation-free transport in type II superconductors. In this paper, we focus on the structural change of a two-dimensional particle system when it is subjected to a periodic potential of different symmetry. We analyze the specific case where the isotropic interaction between particles favors a hexagonal (or equilateral triangular) lattice and subject it to a square substrate lattice with lattice constant b and of varying strength V , fixing the pressure p such as to generate a commensurate density $n = 1/b^2 = (4/3)^{1/2}/a^2$ for the free hexagonal phase. Increasing the substrate potential V , we find the complete pathway of transformations that takes the freely floating hexagonal phase at $V = 0$ to the fully locked square phase at large V .

Effects of discommensuration in periodic external potentials appear in numerous physical systems, promi-

nent examples being atoms on surfaces, e.g., Krypton on graphite³, vortices in modulated superconducting films⁴ and in periodic pinning arrays⁵, flux quanta in Josephson junction arrays⁶, or colloidal monolayers on periodic substrates⁷. Recent applications of such ideas in cold gases are the theoretical analysis of vortex pinning in a Bose-Einstein Condensate subject to an optical lattice^{8,9} or the proposal¹⁰ to realize this physics in a system of dipolar molecules¹¹ subject to a square optical lattice¹²; the high tunability of these cold-gas systems¹³ then can be used to explore the various structural phases. Another recent example is the study of graphene on boron nitride¹⁴ where novel electronic and optical properties can be found.

The original ‘misfit problem’ has been formulated in one dimension (1D) and dealt with a particle lattice with lattice constant a subject to a periodic substrate with incommensurate periodicity $b \neq a$. As shown by Frenkel and Kontorova¹⁵ and by Frank and Van der Merwe¹⁶, the locked system at large potential V (with particle separation b) transforms into the free lattice at $V = 0$ (with separation a between particles) via a smooth commensurate-incommensurate transition. The intermediate non-uniform phase involves solitons with cores approximating the free phase and separating regions of locked phase; the dense soliton array then approaches the free phase with lattice constant a .

The distortion of a two-dimensional particle lattice due to a weak substrate potential has been analyzed by McTague and Novaco¹⁷ within a perturbative (in small V) approach (for lattices with equal symmetry); the distorted lattice becomes orientationally locked to

the substrate at a non-trivial angle φ that depends on the elastic properties of the lattice and on the misfit parameter. Adapting this analysis to our situation, we find a locking angle $\varphi \approx 3.8^\circ$ between the height of the equilateral triangular unit cell and one of the main axes of the substrate potential, see Fig. 1. The commensurate-incommensurate transition in two dimensions (2D) has been first addressed by Pokrovsky and Talapov^{18–20} within the so-called ‘resonance approximation’ where only the leading harmonic of the substrate potential is accounted for. In this situation, the problem reduces to a 1D one and the system develops a secondary structure in the form of an array of soliton-lines. However, with only one substrate harmonic present, the commensurate phase at large potential V is always a rhombic lattice with base $b' > b$ (we call it the bb' rhombic lattice)—in order to obtain the complete pathway connecting the hexagonal and square lattices, both harmonics have to be accounted for.

Rather than starting from the free hexagonal phase and increasing the substrate potential V , it is then more opportune to start from the locked square phase and decrease V . As the square phase is merely stabilized by the large substrate potential, decreasing V naturally generates an instability. It turns out that the leading instability appears at $V_\square \approx 0.2 e_D$ and is given by a shear distortion $\mathbf{u}_{pd} = (0, \delta/2)$ with amplitude δ parallel to the y -axis and a wave vector $\mathbf{q}_{pd} = (\pi/b, 0)$ along x residing at the Brillouin zone boundary (alternatively, the spontaneous symmetry breaking involves a distortion $\mathbf{u}_{pd} = (\delta/2, 0)$ along x with a wavevector $\mathbf{q}_{pd} = (0, \pi/b)$ along y). The resulting zig-zag lattice, see Fig. 1, exhibits a doubled unit cell and has been found before in the context of vortex pinning by a square-lattice pinning potential²¹. Together with the symmetry breaking defining the direction of period-doubling, a second spontaneous symmetry breaking fixes the sign of the amplitude δ , that defines two twin versions of the zig-zag phase. Upon decreasing V further, the amplitude δ of the zig-zag distortion increases, assuming the value $\delta = \pm b/2$, and hence resulting in a rhombic (or isosceles triangular) lattice, at $V = 0$. Although this lattice is close to the hexagonal one, it has the wrong symmetry and hence further transitions are needed to reach the free hexagonal phase.

These transitions are of the commensurate-incommensurate type and the task is to find the most favorable soliton-line appearing first upon decreasing V . While in one dimension only two types of point-solitons either diluting or compressing the particle chain by $\pm b$ are possible, in two dimensions soliton-lines with different ‘topological vector charge’ $\mathbf{d}_{j,k} = (-jb, kb/2)$, j and k mutually prime integers, can be conceived, where the vector charge defines the translation of the lattice on itself or on a twin after the passage of the soliton-line. Thereby, shift vectors $\mathbf{d}_{j,k}$ with odd values of $j+k$ are domain walls connecting unequal twins with $\pm\delta$, while even values of $j+k$ belong to solitons connecting same twins. Out of the

many candidate defects, we find that a dilution-type domain wall (connecting two period-doubled twins) with displacement vector $\mathbf{d}_{01} = (0, b/2)$ is the most favorable defect appearing at the highest value $V_c^{(0,1)} \approx 0.074 e_D$. Quite surprisingly, the domain wall array does not follow one of the symmetry axes of the parent crystal, although such symmetric arrangements have been predicted in the literature²². When domain walls are flooding the lattice upon further decrease in V , they wash out the substrate mode along the y -axis and the particle lattice approaches the bb' rhombic phase resulting from the resonance approximation that neglects just this mode and has been encountered in the discussion further above. The further decrease in V then follows the path described before, with the first Pokrovsky-Talapov type soliton appearing at $V_c^{\text{PT}} \approx 0.046 e_D$ and developing into the distorted and rotated hexagonal phase as the soliton density increases at small V . Note that the vector charge of the Pokrovsky-Talapov soliton-line has only one of its components quantized, $\mathbf{d}^{\text{PT}} = (-b, \delta y)$ with the shift δy along y fixed by the elastic properties of the particle lattice but assuming any (non-quantized) value. The above described rather complex pathway for the square-to-hexagonal transformation involving distorted lattice- as well as non-uniform soliton phases is illustrated in Fig. 1 and is the main result of this paper.

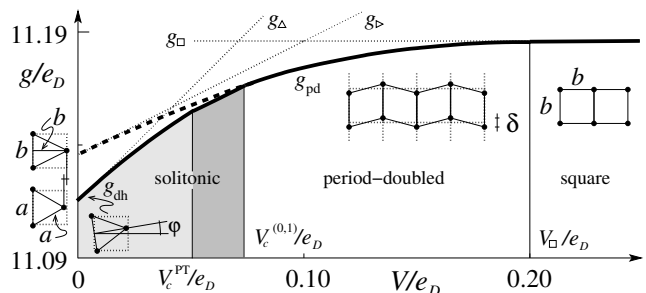


FIG. 1: Gibbs free energy of optimal states (thick line), hexagonal at $V = 0$, distorted and rotated hexagonal (g_{dh}) at small V , solitonic and period-doubled (g_{pd}) at intermediate V , and square for $V > V_\square$. Below the critical potential $V_c^{(0,1)}$, the period-doubled phase smoothly transforms into the hexagonal lattice via two soliton transitions involving different soliton arrays. The dashed line extrapolates the energy g_{pd} of the period-doubled phase. Dotted lines are energies of rigid hexagonal (\triangle), rhombic (\triangleright), and square (\square) configurations.

In the following, we define the model and discuss the rigid lattice approximation (Sec. II) in order to obtain a rough layout of the possible phases and associated energies. We then focus on large values of the substrate potential V : in section III, we find the shear instability in the square lattice and derive a simplified but very accurate model free-energy determining the amplitude δ of the distortion and the energy density g_{pd} of the period-doubled phase, see Fig. 1. In section IV, we analyze

the situation at small substrate potential V^{17} : using the harmonic- and continuum elastic approximations for the hexagonal lattice, we minimize the system's Gibbs free energy as a function of angle φ between the particle- and substrate lattices and determine the optimal value φ_{\min} as well as the associated energy density $g_{\text{dh}}(V)$ of the distorted hexagonal phase. Non-uniform phases are first introduced in section V: increasing V further, the distorted hexagonal phase develops into a soliton phase which we describe in the resonance approximation^{18–20}, dropping the subdominant mode in the substrate potential. We will see, how the soliton array generates a (locally modulated) distortion and rotation that transforms the hexagonal lattice into a bb' rhombic (or isosceles triangular) lattice. Besides understanding the functionality of the soliton phase in transforming the hexagonal lattice to the bb' rhombic one, we are particularly interested in the value of the critical potential V_c for the commensurate-incommensurate transition. The latter can be more easily found by starting from the commensurate phase at higher V and determining the instability for the first soliton entry. In section VI, we calculate the energy of such an individual soliton using the elasticity theory for the bb' rhombic lattice and find the critical substrate potential—the result agrees quite well with the one obtained from the elastic theory for the hexagonal lattice. However, other characteristics such as the soliton direction or soliton amplitude turn out quite different, which we attribute to anharmonicities becoming important in our problem due to the rather large misfit between the hexagonal- and square phases. In order to determine an accurate and reliable value for the critical substrate potential, we solve the particle problem numerically, using the analytic solution as a variational starting point and relaxing the particle positions to find the optimal soliton shape. Section VII deals with the full two-dimensional problem (beyond the resonance approximation): Several candidate solitons and domain walls with different shift vectors $\mathbf{d}_{j,k} = (-jb, kb/2)$ then have to be tested for their critical substrate potential $V_c^{(j,k)}$ —the soliton or domain-wall with the highest V_c will then trigger the transformation away from the period-doubled phase to a non-uniform soliton phase. In order to reach the required precision to separate the critical substrate amplitudes $V_c^{(j,k)}$, the latter have to be determined numerically. Finally, we will establish the transformation pathway in Sec. VIII and conclude in Sec. IX

II. MODEL AND RIGID LATTICE APPROXIMATION

In two dimensions (we consider the $\mathbf{r} = (x, y)$ -plane), particles interacting via a repulsive isotropic two-body potential $\Phi(r)$ arrange in a hexagonal lattice. In this paper, we consider the case of particles with long-range repulsive dipolar interactions $\Phi(\mathbf{r}) = D/r^3$, where $D = d^2$ derives from (electric/magnetic) dipoles \mathbf{d} aligned par-

allel to the z -axis; this situation describes the case of atoms physisorbed on a surface²³, colloidal monolayers⁷, or dipolar molecules in a 2D flat trap¹³. In other cases, e.g., vortex systems^{5,8}, the interaction falls off logarithmically, changing the numerical values of the results in the analysis described below—however, we expect that such systems exhibit a similar overall behavior.

We submit this particle-system to a periodic lattice, in our case a square periodic lattice with lattice constant b and amplitude V . Such a substrate lattice (possibly of another, e.g., hexagonal, symmetry) appears naturally in the case of physisorption on a surface³ or is artificially imposed with the help of optical tweezers⁷, optical lattices¹³, or pinning arrays⁵. We consider the case where thermal and quantum fluctuations are negligible; this situation is described through the Hamiltonian or total energy E for N particles confined within an area A ,

$$\begin{aligned} E(A, N) &= E^{\text{int}} + E^{\text{sub}} \\ &= \frac{1}{2} \sum_{i \neq j} \frac{D}{r_{ij}^3} + \frac{V}{2} \sum_{i, \alpha} [1 - \cos(\mathbf{q}_\alpha \cdot \mathbf{r}_i)], \end{aligned} \quad (1)$$

where particles are located at positions \mathbf{r}_i with distances $r_{ij} \equiv |\mathbf{r}_i - \mathbf{r}_j|$; the substrate potential involves the two modes $\mathbf{q}_1 = (q, 0)$ and $\mathbf{q}_2 = (0, q)$ with $q = 2\pi/b$ along the x - and y -axis.

A crucial parameter is the particle density $n = N/A$ determining the lattice constant $a = (4/3n^2)^{1/4}$ of the hexagonal lattice. We choose to work at fixed pressure p , which is arranged in such a way as to define a commensurate density $n = 1/b^2$ at $V = 0$, i.e., for the free hexagonal phase; the change to a situation with a fixed chemical potential μ is straightforward. For a large potential V , the particles fit the minima of the substrate potential (hence again $n = 1/b^2$), however, the density will change, in fact decrease, at intermediate values of V . The misfit parameter s between the hexagonal and square lattices is determined by the distance between rows in the hexagonal (the height $h = \sqrt{3}/4a$) and in the square lattice (the lattice constant b),

$$s = \frac{b}{h} - 1 \approx 0.0746, \quad (2)$$

and corresponds to a lattice constant a of the hexagonal lattice that is slightly larger than that of the substrate lattice, $a = (4/3)^{1/4}b > b$. Note that large misfits s potentially create large lattice distortions, what may turn out problematic in the use of the harmonic approximation; we will see below that our misfit parameter of order ~ 0.1 is quite large in this respect.

Working at fixed pressure p , the appropriate potential to minimize is the Gibbs free energy $G(p, N)$: starting with the system's energy (1) for N particles trapped within the area A , the Legendre transform with $\partial_A E = -p$ provides us with the Gibbs free energy per particle

$$g(p) = G(p, N)/N = [E(A, N) + pA]/N, \quad (3)$$

where the thermodynamic limit $N, A \rightarrow \infty, n = N/A = \text{const.}$ is implied.

In the rigid lattice approximation, we fix lattice sites \mathbf{R}_j and determine the Gibbs free energy density g via straightforward summation. The long-range potential in the interaction energy density e^{int} is conveniently handled with an Ewald²⁴ summation technique (see appendix A), splitting the sum in Eq. (1) into two terms describing near and distant particles through real- and reciprocal space contributions,

$$\begin{aligned} e^{\text{int}} &= \pi e_D \left\{ \frac{4}{3} + \sum_{j \neq 0} [\Psi_{\frac{1}{2}}(\epsilon R_j^2) + \Psi_{-\frac{3}{2}}(K_j^2/4\epsilon)] \right\} \\ &= \pi e_D \left\{ \frac{4}{3} + \sum_{j \neq 0} [\Psi_{\frac{1}{2}}(\pi n R_j^2) + \Psi_{-\frac{3}{2}}(\pi n R_j^2)] \right\}, \end{aligned} \quad (4)$$

where we have chosen an Ewald parameter^{24–26} $\epsilon = \pi n$ and have used the property $K_j^2 = (2\pi n)^2 R_j^2$ in the last equation. Here, $\Psi_x(\beta) = \beta^{-(x+1)} \Gamma(x+1, \beta)$ with $\Gamma(x, \beta)$ the incomplete Gamma function, \mathbf{K}_j are reciprocal lattice sites, and $e_D = Dn^{3/2} = D/b^3$ is the dipolar energy scale.

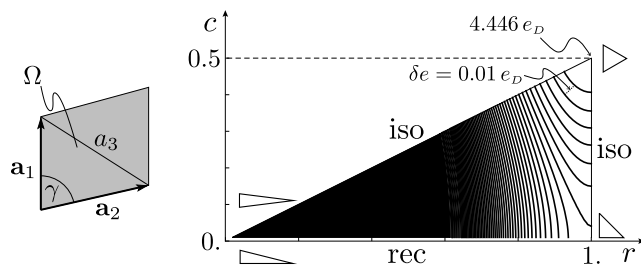


FIG. 2: Left: Parametrization of 2D Bravais lattices with given unit cell area $\Omega = b^2$. The lattice vectors \mathbf{a}_1 and \mathbf{a}_2 are chosen such that $a_1 < a_2 < a_3$ and γ is the angle enclosed by \mathbf{a}_1 and \mathbf{a}_2 . Right: The region $0 < r = a_1/a_2 < 1$, $0 \leq c = \cos \gamma \leq r/2$ uniquely covers all possible Bravais lattices. Boundaries correspond to rectangular unit cells and isosceles triangles (rhombic lattices), respectively. The contours mark constant energy lines, with the lowest energy $e_\Delta \approx 4.446 e_D$ attained for the hexagonal or equilateral triangular lattice. The square lattice assumes a saddle-point configuration. Lines start at e_Δ and are separated by $0.01 e_D$.

Parametrizing the 2D Bravais lattices by the lattice vectors \mathbf{a}_1 and \mathbf{a}_2 with $a_1 \leq a_2 \leq a_3$ via the length ratio $r = a_1/a_2$ and the angle γ enclosed between the two (shortest) vectors \mathbf{a}_1 and \mathbf{a}_2 , we can describe all lattices by choosing values $0 < r \leq 1$ and $0 \leq c = \cos \gamma \leq r/2$, see Fig. 2. The latter boundary derives from the condition $a_3^2 = a_1^2 + a_2^2 - 2a_1 a_2 \cos \gamma \geq a_2^2$ with $\cos \gamma > 0$ (a situation with $\gamma > \pi/2$ can be reduced to the triangular region in the c - r diagram by choosing another lattice vector). The interaction energy e^{int} per particle for the different lattices is shown in the contour plot of Fig. 2. As expected, the minimal energy is assumed by the hexagonal lattice with $e_\Delta \approx 4.446 e_D$, but other configurations

such as the rhombic lattice with height b ($e_\triangleright \approx 4.467 e_D$) or the square lattice (with $e_\square \approx 4.517 e_D$) are close-by in energy.

Minimizing the Gibbs free energy $g(p, n) = e_\Delta(n) + p/n$ at $V = 0$ with respect to the density n provides us with the expression for the pressure²⁷

$$p = \frac{3}{2} n e_\Delta(n). \quad (5)$$

In the following, we will fix the pressure p to generate the density $n = 1/b^2$ at $V = 0$; when increasing the substrate potential V at this fixed value of p , the density will change and return back to the value $n = 1/b^2$ at larger V in the period-doubled and square phases. Note that with a purely repulsive interaction it is the pressure p which determines the lattice constant a , i.e., the hexagonal lattice has no own ‘generic’ lattice constant, see also the discussion in appendix C.

When calculating the substrate energy in a rigid lattice approximation, we encounter three classes with the following substrate energies per particle, depending whether none, one, or two substrate modes line up with the particle positions,

$$e^{\text{sub}}(V) = \begin{cases} V & \mathbf{q}_1, \mathbf{q}_2 \notin \{\mathbf{K}_j\}, \\ V/2 & \mathbf{q}_1 \text{ or } \mathbf{q}_2 \in \{\mathbf{K}_j\}, \\ 0 & \mathbf{q}_1, \mathbf{q}_2 \in \{\mathbf{K}_j\}, \end{cases} \quad (6)$$

where $\{\mathbf{K}_j\}$ denotes the set of reciprocal lattice vectors of the particle lattice with sites $\{\mathbf{R}_i\}$. This follows from the sum

$$\begin{aligned} e^{\text{sub}}(\mathbf{d}) &= \frac{1}{N} \sum_{i=1}^N V^{\text{sub}}(\mathbf{R}_i + \mathbf{d}) \\ &= \frac{V}{2} \sum_{\alpha=1,2} \left[1 - \cos(\mathbf{q}_\alpha \cdot \mathbf{d}) \left(\sum_j \delta_{\mathbf{K}_j, \mathbf{q}_\alpha} \right) \right], \end{aligned} \quad (7)$$

where changes in the translational shift \mathbf{d} quantify the locking energy of the rigid lattice.

Combining the results for the interaction and substrate energies as well as the pressure p , we find three favorable configurations, hexagonal (unlocked), rhombic with base b and height b (single locked²⁸, below called the bb -lattice), and square (double locked) with Gibbs free energies $g(V) = e^{\text{int}} + p/n + e^{\text{sub}}(V)$,

$$\begin{aligned} g_\Delta(V) &= g_\Delta + V \approx 11.115 e_D + V, \\ g_\triangleright(V) &= g_\triangleright + V/2 \approx 11.136 e_D + V/2, \\ g_\square &\approx 11.186 e_D. \end{aligned} \quad (8)$$

Note that in choosing the orientation of the bb -lattice we have to break the symmetry of the system spontaneously—this symmetry breaking is triggered by the shear instability of the square phase leading to the period-doubled phase as described in Sec. III below. The above expressions for $g_\Delta(V)$, $g_\triangleright(V)$, and g_\square already provide a reasonable approximation to the energy g versus potential V diagram as illustrated in Fig. 1 (dotted lines).

III. PERIOD-DOUBLED PHASE

Going beyond the rigid lattice approximation, we account for small deviations \mathbf{u}_i of the particle coordinates $\mathbf{r}_i = \mathbf{R}_i^{\text{latt}} + \mathbf{u}_i$ from regular lattice positions $\mathbf{R}_i^{\text{latt}}$. The harmonic expansion of the energy (1) in the displacement field \mathbf{u}_i provides us with corrections to the Gibbs free energy $g = g_{\text{latt}} + \delta g$. The interaction energy $g^{\text{int}} = e^{\text{int}} + p/n$ contributes a term

$$\delta g^{\text{int}} \approx \frac{1}{2N} \sum_{i,j} u_{i\mu} \Phi_{\mu\nu}^D(\mathbf{R}_{ij}^{\text{latt}}) u_{j\nu}, \quad (9)$$

with the elastic matrix $\Phi_{\mu\nu}^D(\mathbf{R}_{ij}^{\text{latt}})$ depending on the chosen lattice, while the substrate potential adds a second

term δe^{sub} to δg , $\delta g = \delta g^{\text{int}} + \delta e^{\text{sub}}$. For a dipolar system, the elastic matrix assumes the form

$$\Phi_{\mu\nu}^D(\mathbf{R}_{ij}) = D(1 - \delta_{ij}) \left[3 \frac{\delta_{\mu\nu}}{R_{ij}^5} - 15 \frac{\mathbf{R}_{ij,\mu} \mathbf{R}_{ij,\nu}}{R_{ij}^7} \right] - D\delta_{ij} \sum_{l,l \neq i} \left[3 \frac{\delta_{\mu\nu}}{R_{il}^5} - 15 \frac{\mathbf{R}_{il,\mu} \mathbf{R}_{il,\nu}}{R_{il}^7} \right]. \quad (10)$$

Its Fourier transform²⁹ $\Phi_{\mu\nu}^D(\mathbf{k}) = \sum_j \Phi_{\mu\nu}^D(\mathbf{R}_{ij}) \exp(-i\mathbf{k} \cdot \mathbf{R}_{ij})$ is conveniently calculated with the help of the Ewald summation technique,²⁴

$$\begin{aligned} \Phi_{\mu\nu}^D(\mathbf{k}) = & 4\pi^2 D n^{5/2} \left\{ \frac{k_\mu k_\nu}{2\epsilon} \Psi_{-\frac{3}{2}}(k^2/4\epsilon) + \sum_{j \neq 0} \left[2\epsilon R_{j\mu} R_{j\nu} \Psi_{\frac{5}{2}}(\epsilon R_j^2) - \delta_{\mu\nu} \Psi_{\frac{3}{2}}(\epsilon R_j^2) \right] [1 - \cos(\mathbf{k} \cdot \mathbf{R}_j)] \right. \\ & \left. + \sum_{j \neq 0} \left[\frac{(K_{j\mu} - k_\mu)(K_{j\nu} - k_\nu)}{2\epsilon} \Psi_{-\frac{3}{2}}(|\mathbf{K}_j - \mathbf{k}|^2/4\epsilon) - \frac{K_{j\mu} K_{j\nu}}{2\epsilon} \Psi_{-\frac{3}{2}}(K_j^2/4\epsilon) \right] \right\} \end{aligned} \quad (11)$$

with \mathbf{k} residing in the first Brillouin zone. Determining the eigenvectors $\mathbf{e}_{\mathbf{k}}^\nu$ and eigenvalues $\phi_{\mathbf{k}}^\nu$ allows for a stability analysis of the lattice $\mathbf{R}_i^{\text{latt}}$ under small local distortions. E.g., evaluating the eigenvalues along the high symmetry directions in the Brillouin zone for the hexagonal lattice $\mathbf{R}_i^{\text{latt}} = \mathbf{R}_i^\Delta$ one finds positive transverse ($\nu = \perp$) and longitudinal ($\nu = \parallel$) eigenvalues, see Fig. 3; in the long-wavelength limit, these are the usual compression and shear modes (see also appendix C 1)

$$\begin{aligned} \mathbf{e}_{\mathbf{k}}^\parallel &= (k_x, k_y)/k, & \phi_{\mathbf{k}}^\parallel &\approx [(\kappa + \mu)/n] k^2, \\ \mathbf{e}_{\mathbf{k}}^\perp &= (k_y, -k_x)/k, & \phi_{\mathbf{k}}^\perp &\approx (\mu/n) k^2, \end{aligned} \quad (12)$$

with

$$\mu = \frac{3}{8} n e_\Delta, \quad \kappa = \frac{15}{4} n e_\Delta, \quad (13)$$

the shear and compression moduli of the isotropic (at small k) hexagonal lattice.

For a large substrate potential V , the substrate enforces a square lattice with particle positions $\mathbf{R}_i^{\text{latt}} = \mathbf{R}_i^\square$. Evaluating the elastic matrix $\Phi_{\mu\nu}^D(\mathbf{k})$ in Eq. (11) for \mathbf{k} within the first Brillouin zone and determining its eigenvalues, we find an unstable branch with the largest negative eigenvalue appearing at the X -point assuming a numerical value $\phi^\perp(0, \pi/b) = -3.958 e_D n$, see Fig. 4. On the other hand, the substrate potential contributes a term $\delta e^{\text{sub}} \approx V q^2 |u_{\mathbf{k}}|^2/2$ to the free energy correction δg , pushing up the entire spectrum. Including this upward shift, all modes remain stable for $V > V_\square$ with the

critical value for the potential V_\square defined by the equation

$$\frac{q^2}{2} V_\square = |\phi^\perp(0, \pi/b)| = 3.958 e_D n, \quad (14)$$

hence

$$V_\square = 0.201 e_D. \quad (15)$$

At $V = V_\square$ the lowest eigenvalue of $\Phi_{\mu\nu}^D(\mathbf{k})$ touches zero at the X -points $(\pi/b, 0)$ and $(0, \pi/b)$ and the lattice deforms, with a shear mode doubling the unit cell in one of the two principal directions x or y ; the two possible choices for this zig-zag distortion correspond to a \mathbb{Z}_2 -symmetry breaking. Furthermore, for each choice of principal direction x or y , the sign of the distortion $\delta/2$ can be

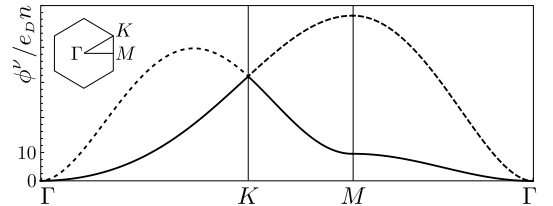


FIG. 3: Transverse (lower branch) and longitudinal (upper branch) eigenvalues for the hexagonal lattice along symmetry axes as calculated using Eq. (11). For small wavevectors k around the Γ -point, $\phi_{\mathbf{k}}^\perp \approx (\mu/n) k^2$ and $\phi_{\mathbf{k}}^\parallel \approx [(\kappa + \mu)/n] k^2$ describe shear and compression modes.

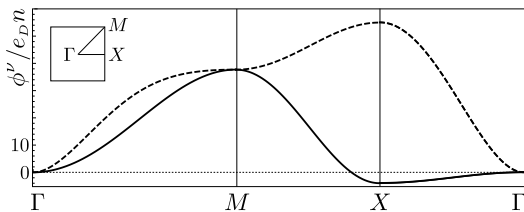


FIG. 4: Transverse (lower branch) and longitudinal (upper branch) eigenvalues for the square lattice along high symmetry axes as calculated using Eq. (11). The transverse branch becomes negative along the line $\Gamma - X - M$, indicating an instability of the square lattice. The presence of the square substrate potential lifts these eigenvalues to stabilize them above a threshold V_\square .

reversed, defining two twins as shown in Fig. 5(a) (alternatively, the sign change in the distortion can be viewed as a shift by b).

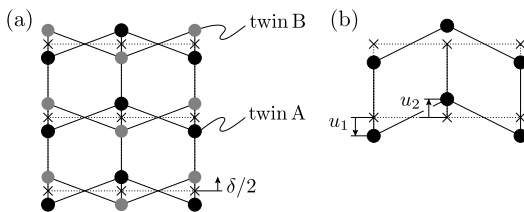


FIG. 5: The two possible zig-zag structures for an instability at the X -point $(\pi/b, 0)$. The crosses represent the undistorted square lattice, whereas the black and dark grey points show the twins A and B, respectively. The twin structures transform into one another either by changing the sign of the distortion $\delta/2$ or by a shift by b along x .

A. Period-doubled phase relative to the square lattice

Next, we determine the amplitude δ of the zig-zag distortion in the period-doubled phase for $V < V_\square$ assuming an instability realized at $X = (\pi/b, 0)$. We start from the square lattice and consider a rectangular unit cell with lattice vectors $\mathbf{a}_1^R = (2b, 0)$ and $\mathbf{a}_2^R = (0, b)$ holding two particles at positions $\mathbf{c}_1 = (0, u_1)$ and $\mathbf{c}_2 = (b, u_2)$, see Fig. 5(b). Defining center-of-mass and difference coordinates

$$\sigma = (u_1 + u_2)/2, \quad \delta = u_1 - u_2, \quad (16)$$

we determine the interaction energy of the period-doubled phase choosing a reference frame shifted by $\delta/2$,

$$e_{\text{pd}}^{\text{int}}(\delta) = \frac{1}{2} \sum_{j=1}^{N/2} \frac{D}{(R_j^R)^3} + \frac{1}{2} \sum_{j=1}^{N/2} \frac{D}{|\mathbf{R}_j^R + \mathbf{c}|^3} \quad (17)$$

with the shift $\mathbf{c} = (b, \delta)$. The first sum is the energy of the rectangular lattice and is evaluated with an Ewald summation to provide the energy per particle $e_{\text{R}}^{\text{int}} = 2.025 e_D$. The second sum is decomposed into a sum over columns (index l) and rows (index m); applying the Poisson summation rule to the sum over l , Eq. (17) can be rewritten as (see appendix B)

$$e_{\text{pd}}^{\text{int}}(\delta) = e_{\text{R}}^{\text{int}} + \frac{\pi^2}{4} e_D \quad (18)$$

$$+ 8\pi e_D \sum_{m>0} \sum_{l>0} \frac{l' K_1[2\pi l'(2m-1)]}{2m-1} \cos(q l' \delta),$$

where l' accounts for the particle rows in reciprocal space; the term $l' = 0$ has been treated separately and contributes the energy $(\pi^2/4) e_D$. The modified Bessel function of the second kind $K_1(z)$ decays rapidly, $K_1(z) \propto e^{-z}$, such that we can discard terms with $l' > 1$ and $m > 1$; the interaction energy per particle then takes the simple form

$$e_{\text{pd}}^{\text{int}}(\delta) \approx e_{\text{R}}^{\text{int}} + \frac{\pi^2}{4} e_D + 8\pi e_D K_1[2\pi] \cos(q\delta) \quad (19)$$

$$\equiv C_1 + C_2 \cos(q\delta)$$

with the constants $C_1 = 4.492 e_D$ and $C_2 = 0.0248 e_D$. Going over to the Gibbs energy by adding the pressure term $p/n = 3e_\Delta/2$ and rearranging terms, we obtain

$$g_{\text{pd}}^{\text{int}}(\delta) = g_\triangleright + \Delta [1 + \cos(q\delta)] \quad (20)$$

with

$$\Delta = \frac{g_\square - g_\triangleright}{2} = 0.0248 e_D. \quad (21)$$

It is easily seen that the ‘asymptotic cases’ are in agreement with our expectations, i.e., $g_{\text{pd}}^{\text{int}}(\delta = 0) = g_\square$ and $g_{\text{pd}}^{\text{int}}(\delta = \pm b/2) = g_\triangleright$. The interaction energy (20) differs from the exact result obtained by the Ewald method by far less than a per mill such that the approximation made in the step going from (18) to (19) is well-justified.

The substrate potential e^{sub} contributes a term

$$e_{\text{pd}}^{\text{sub}}(V, \sigma, \delta) = \frac{V}{2N} \sum_j [2 - \cos(qu_1) - \cos(qu_2)]$$

$$= \frac{V}{2} [1 - \cos(q\sigma) \cos(q\delta/2)], \quad (22)$$

where the sum over j goes over $N/2$ particles. Minimizing the Gibbs free energy $g_{\text{pd}} = g_{\text{pd}}^{\text{int}} + e_{\text{pd}}^{\text{sub}}$ with respect to the distortion δ , we find the latter related to the center-of-mass coordinate σ via

$$\cos(q\delta/2) = \frac{V}{8\Delta} \cos(q\sigma) \quad (23)$$

and obtain the energy of the period-doubled phase

$$g_{\text{pd}}(V, \sigma) = g_\triangleright + \frac{V}{2} - \frac{V^2}{32\Delta} + \frac{V^2}{64\Delta} [1 - \cos(2q\sigma)], \quad (24)$$

with the distortion δ slaved to σ . This slaved distortion generates the period-halving $b/2$ and a small periodic energy $V^2/32\Delta$ for the motion of the particle lattice along the y axis (by increasing σ), hence the period-doubled phase is pinned to the substrate with respect to both directions x and y , although much weaker along the y -axis. Minimal energy configurations are realized for $\sigma = nb/2$, $n \in \mathbb{Z}$. Choosing the solution $\sigma = 0$ (or 2σ equal to an even multiple of b), Eq. (23) provides us with the distortion amplitude

$$\delta(V) = \frac{b}{\pi} \arccos(V/8\Delta), \quad (25)$$

where both signs of the arccos are relevant; the sign of δ then decides into which of the two degenerate zig-zag solutions $u_1 = -u_2 = \delta/2$ the system deforms, see Fig. 5 ($\delta < 0$ for twin A). The condition $\delta = 0$ provides us with an alternative result for the critical potential $V_\square = 8\Delta \approx 0.198 e_D$; this value is close to the previous result (15), again confirming that terms with $m > 1$ or $l' > 1$ in Eq. (18) are indeed small. The order parameter approaches zero as $\delta \approx \pm(\sqrt{2}b/\pi)\sqrt{1 - V/V_\square}$ on approaching the square lattice, while $\delta = \pm(b/2)[1 - 2V/\pi V_\square]$ near $V = 0$ describes the vicinity of the bb rhombic lattice with energy g_\triangleright , see Fig. 6. When approaching the state with maximal distortion amplitude $\pm b/2$ at $V = 0^+$ the particles assume the symmetric positions between the potential maxima and minima along y . The energy of the period-doubled phase

$$g_{\text{pd}}(V) = g_\triangleright + \frac{V}{2} - \frac{V^2}{32\Delta} \quad (26)$$

undercuts that of the rigid phase approximation and smoothly interpolates between the energy g_\triangleright of the bb rhombic lattice at $V = 0$ and the energy $g_\square = g_\triangleright + 2\Delta$ of the square lattice at $V_\square = 8\Delta$, see Fig. 1.

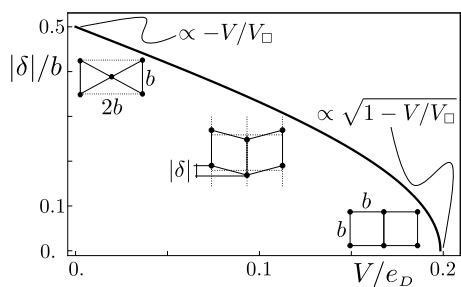


FIG. 6: The relative distortion $|\delta|$ assumes its maximal value $b/2$ in the bb rhombic phase at $V = 0$, decreases $\propto V/V_\square$ for small substrate amplitudes, and goes to zero $\propto \sqrt{1 - V/V_\square}$ as V approaches V_\square .

Equivalent solutions (involving the branch of arccos around 0) are obtained for $2\sigma = nb$ with even n (although the displacements u_1 and u_2 are no longer antisymmetric). Care has to be taken when choosing $2\sigma = nb$ with

an odd integer n ; in this case, the right hand side of Eq. (23) is negative and the solutions for δ involve the branches of arccos around $\pm\pi$.

B. Period-doubled phase relative to the bb rhombic lattice

In the analysis above, we have described the period-doubled phase as it develops out of the square phase under a shear distortion that is increasing with decreasing substrate amplitude V . On the other hand, when studying the instability of the period-doubled phase towards formation of topological defects (soliton- or domain-wall lines, see Sec. VII) a description with reference to the bb rhombic phase is more convenient. Defining the displacements \bar{u}_1 and \bar{u}_2 with respect to the latter, we define the positions of the particles in the rectangular unit cell via $\bar{\mathbf{c}}_1 = (0, \bar{u}_1)$ and $\bar{\mathbf{c}}_2 = (b, b/2 + \bar{u}_2)$ and determine once more the interaction and substrate energies of the distorted phase,

$$g_{\text{pd}}^{\text{int}}(\bar{\delta}) = g_\triangleright + \Delta[1 - \cos(q\bar{\delta})] \quad (27)$$

and

$$e^{\text{sub}}(V, \bar{\sigma}, \bar{\delta}) = \frac{V}{2} \{1 + \sin(q\bar{\sigma}) \sin(q\bar{\delta}/2)\}, \quad (28)$$

where $\bar{\sigma} = (\bar{u}_1 + \bar{u}_2)/2$ and $\bar{\delta} = \bar{u}_1 - \bar{u}_2$. Minimizing the total free energy with respect to $\bar{\delta}$ we obtain

$$\sin(q\bar{\delta}/2) = -\frac{V}{8\Delta} \sin(q\bar{\sigma}) \quad (29)$$

and the energy

$$g_{\text{pd}}(V, \bar{\sigma}) = g_\triangleright + \frac{V}{2} - \frac{V^2}{32\Delta} + \frac{V^2}{64\Delta} [1 + \cos(2q\bar{\sigma})]. \quad (30)$$

Minima now are located at $2\bar{\sigma} = b(2n + 1)/2$, $n \in \mathbb{Z}$, in agreement with the results above as $\bar{\sigma} = \sigma - b/4$. Choosing $n = -1$, $\bar{\sigma} = -b/4$ provides us with the identical particle positions as before when starting from the square phase: The relative distortion $\bar{\delta} = \delta + b/2$ grows from $\bar{\delta} = 0$ at $V = 0^+$ (twin A solution, see Fig. 7) to $\bar{\delta} = b/2$ (square lattice) as $V \rightarrow 8\Delta$,

$$\bar{\delta}(V) = (b/\pi) \arcsin(V/8\Delta). \quad (31)$$

On returning back to $V = 0^+$, we can follow the same path or choose another branch of the arcsin-function that has $\bar{\delta}$ increase further, generating the twin B solution on returning back to $V = 0^+$, see Fig. 7. Note that the negative branch of the arcsin is not compatible with Eq. (29) and $\bar{\sigma} = -b/4$. Instead, the alternative twin phase, previously realized by changing the sign of δ , is now conveniently encoded through a change in the center-of-mass coordinate by going over to the value $\bar{\sigma} = b/4$, see Fig. 7. Below, we will find domain walls defined through shifts of the lattice along y , i.e., by increasing $\bar{\sigma}$ by one

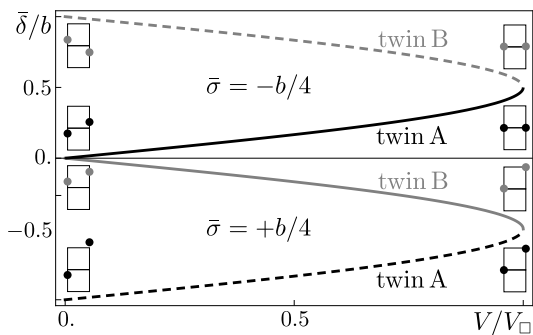


FIG. 7: The twin-B phase may be reached from the twin-A phase by changing the center-of-mass coordinate $\bar{\sigma}$ from $\bar{\sigma} = -b/4$ to $\bar{\sigma} = b/4$.

period $b/2$ from one minimum in the energy $g_{\text{pd}}(V, \bar{\sigma})$ to the next, see Eq. (30). When pushing the center-of-mass coordinate $\bar{\sigma}$ from $-b/4$ to $b/4$, the slaved distortion $\bar{\delta}$ will transit through zero (where the lattice has the bb rhombic geometry) and connect the twin A with the twin B phase.

IV. LOCKED HEXAGONAL PHASE

Next, we focus our interest on weak substrate potentials V . Going again beyond the rigid lattice approximation, the lattice will deform and the particle positions will deviate away from regular hexagonal lattice positions, i.e., in Eq. (1) we choose $\mathbf{R}_i^{\text{latt}} = \mathbf{R}_i^\Delta$ and $\mathbf{r}_i = \mathbf{R}_i^\Delta + \mathbf{u}_i$. At $V = 0$ the position and orientation of the floating hexagonal lattice is arbitrary; without loss of generality, we can fix the point \mathbf{R}_0^Δ in a substrate minimum coming up at finite $V > 0$, e.g., $\mathbf{R}_0^\Delta = (0, 0)$. At finite but small V , the particle lattice will relax and optimize its energy. This optimization depends on the relative orientation φ , the angle enclosing the x -axis and the height of a triangle as shown in Fig. 1. Our task then is to find the optimal angle providing the largest energy relaxation. At small values of V , the displacements \mathbf{u}_i remain small, $u_i \ll a$ for all i , and the change in the interaction energy of Eq. (1) can be calculated in a harmonic approximation using $\delta g_\Delta^{\text{int}}$, see Eq. (9). Expanding the substrate potential to linear order in the displacement¹⁷, we obtain the contribution

$$\delta e_\Delta^{\text{sub}} \approx \frac{1}{N} \sum_i \mathbf{u}_i \cdot \mathbf{f}_i^{\text{sub}} \quad \text{with} \quad (32)$$

$$\mathbf{f}_i^{\text{sub}} = \frac{V}{2} \sum_\alpha \mathbf{q}_\alpha \sin[\mathbf{q}_\alpha \cdot \mathbf{R}_i^\Delta] \quad (33)$$

to the system's free energy correction δg_Δ . The minimization of the Gibbs free energy $\delta g_\Delta = \delta g_\Delta^{\text{int}} + \delta e_\Delta^{\text{sub}}$ with respect to the displacement field \mathbf{u}_i is conveniently done in Fourier space³⁰ and we obtain the solution

$$\mathbf{u}(\mathbf{k}) = -[\hat{\Phi}^D]^{-1}(\mathbf{k}) \mathbf{f}^{\text{sub}}(\mathbf{k}), \quad (34)$$

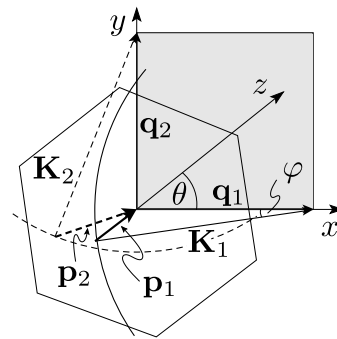


FIG. 8: Sketch of the reduction of the substrate's \mathbf{q}_1 - and \mathbf{q}_2 -vectors back to the first Brillouin zone of the (rotated hexagonal) particle lattice. The back-folded \mathbf{q} -vectors \mathbf{p}_1 and \mathbf{p}_2 assume values on circular segments; these segments derive from different sectors of circles of radii K_1 and K_2 around \mathbf{q}_1 and \mathbf{q}_2 which emerge when rotating the particle lattice against the fixed substrate (angle φ). A small value of \mathbf{p}_1 or \mathbf{p}_2 provides a large relaxation energy. For later use, the z -axis pointing along \mathbf{p}_1 and enclosing an angle θ with the x -axis is also shown.

with $\hat{\Phi}^D(\mathbf{k})$ the Fourier transform of the elastic matrix $\hat{\Phi}^D(\mathbf{R}_{ij}^\Delta)$ and \mathbf{k} belonging to the first Brillouin zone of the (φ -rotated) hexagonal lattice. The force field³¹ $\mathbf{f}^{\text{sub}}(\mathbf{k}) = (VN/4i) \sum_\alpha (\delta_{\mathbf{k}, -\mathbf{p}_\alpha} - \delta_{\mathbf{k}, \mathbf{p}_\alpha}) \mathbf{q}_\alpha$ involves the two modes \mathbf{q}_α , $\alpha = 1, 2$, of the substrate potential, folded back to the first Brillouin cell of the particle lattice, see Fig. 8, $\mathbf{q}_\alpha - n_\alpha \mathbf{K}_1 - m_\alpha \mathbf{K}_2 \equiv -\mathbf{p}_\alpha$, with $\mathbf{K}_1, \mathbf{K}_2$ the reciprocal lattice vectors of the (rotated hexagonal) particle lattice, n_α, m_α are appropriate integers, and we have included a minus sign in the definition of \mathbf{p}_α for convenience.

Inserting the solution for the displacement field back into the expression for the free energy relaxation, we obtain the result

$$\delta g_\Delta(V, \varphi) = -\frac{\pi^2}{4} n V^2 \{ [\hat{\Phi}^D]_{11}^{-1}(\mathbf{p}_1) + [\hat{\Phi}^D]_{22}^{-1}(\mathbf{p}_2) \}, \quad (35)$$

where the dependence on the angle φ is encoded in the misfit vectors \mathbf{p}_α , see Fig. 8. Calculating $\hat{\Phi}^D(\mathbf{k})$ with the help of Eq. (11) and evaluating the energy relaxation $\delta g_\Delta(V, \varphi)$ as a function of φ , see Fig. 9, we find the locking angle

$$\varphi_{\text{min}} \approx \pm 3.83^\circ \quad (36)$$

minimizing the free energy of the distorted hexagonal lattice. Corrections to this result are of order V^2 and require to go beyond the harmonic approximation.

Instead of a numerical minimization of the free energy, one can make use of the *resonance approximation* that includes only the dominant mode in the substrate potential^{19,20}. Rotating the hexagonal particle lattice with respect to the square substrate potential, the misfit vectors \mathbf{p}_α move on arcs through the Brillouin zone, see Fig. 8. For a small misfit parameter s , one of the \mathbf{p}_α

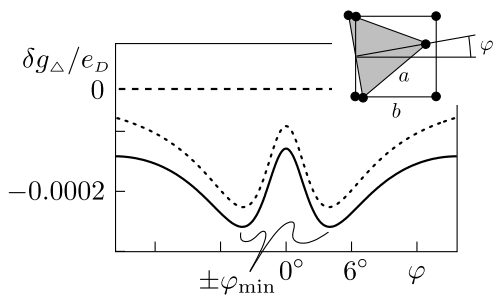


FIG. 9: Lowering of the free energy due to particle relaxation as a function of relative orientation φ between the particle lattice and the substrate for a small substrate amplitude $V = 0.01 e_D$. The maximal energy gain is reached at $\varphi_0 \approx \pm 3.83^\circ$ and leads to an orientational locking of the particle lattice. The dotted line is the result of the resonance approximation, the dashed line marks the energy without relaxation.

passes near zero, inducing a large relaxation (and accordingly a large energy gain) as the elastic matrix becomes soft with small eigenvalues, see Eq. (12). Within the resonance approximation^{19,20}, only the dominant term in the relaxation deriving from the small misfit vector, say $\mathbf{p}_1 = \mathbf{K}_1 - \mathbf{q}_1$, is included, while the small correction due to the other mode is dropped; in the following, we drop the index 1 on \mathbf{q}_1 , \mathbf{K}_1 , and \mathbf{p}_1 . A similar approximation has been used by McTague and Novaco¹⁷ when calculating the accommodation of a hexagonal lattice to a substrate with the same (hexagonal) symmetry but with a different lattice constant. Adopting the long-wavelength approximation (12), the expression (35) for the energy relaxation simplifies considerably,

$$\delta g_\Delta(V, \varphi) \approx -\frac{V^2}{16} \sum_\lambda \frac{1}{\phi_\mathbf{p}^\lambda} [\mathbf{e}_\mathbf{p}^\lambda \cdot \mathbf{q}]^2, \quad (37)$$

where $\mathbf{e}_\mathbf{p}^\parallel = \mathbf{p}/p$ and $\mathbf{e}_\mathbf{p}^\perp = \mathbf{p}^\perp/p$. With $\mathbf{e}_\mathbf{p}^\parallel \cdot \mathbf{q} = q \cos \theta$ and $\mathbf{e}_\mathbf{p}^\perp \cdot \mathbf{q} = q \sin \theta$, see Fig. 8, and using the law of sines $K/\sin \theta = p/\sin \varphi$, we arrive at the simple result

$$\delta g_\Delta(V, \varphi) = -\frac{nV^2}{16(\kappa + \mu)} \frac{q^2}{p^2} \left[1 + \frac{\kappa}{\mu} \frac{K^2}{p^2} \sin^2 \varphi \right]. \quad (38)$$

The first term favors a minimal modulus p at $\varphi = 0$, while the second term favors a finite angle φ . Replacing $p^2 = q^2 + K^2 - 2qK \cos \varphi$ and defining $r = K/q = 1 + s$, this can be rewritten as

$$\delta g_\Delta(V, \varphi) = -\frac{nV^2}{16(\kappa + \mu)} \left[\frac{1}{1 + r^2 - 2r \cos \varphi} + \frac{\kappa}{\mu} \left(\frac{r \sin \varphi}{1 + r^2 - 2r \cos \varphi} \right)^2 \right] \quad (39)$$

and the minimization of this expression with respect to φ provides us with the optimal angle φ_{\min} given through

$$\cos \varphi_{\min} = 1 - s^2 \frac{r - \mu/\kappa}{r(1 + r^2 + 2\mu/\kappa)}. \quad (40)$$

Expanding this result for small φ_{\min} and small s we obtain the final answer

$$\varphi_{\min} = s\sqrt{\nu} \approx 3.86^\circ \quad (41)$$

with $\nu = (\kappa - \mu)/(\kappa + \mu)$ the Poisson ratio and we have made use of the elastic constants in Eq. (13). Within the same accuracy (i.e., to leading order in s), we find the misfit vector

$$\mathbf{p} = sq \begin{pmatrix} 1 \\ \sqrt{\nu} \end{pmatrix} \quad (42)$$

enclosing an angle

$$\theta = \arctan \sqrt{\nu} \approx 42.13^\circ \quad (43)$$

with the x -axis, see Fig. 8. The displacement field \mathbf{u} evolves periodically along \mathbf{p} (or z , see Fig. 8)

$$\mathbf{u}(\mathbf{R}) = \frac{b}{8\pi s^2} \frac{nV}{\mu\sqrt{1+\nu}} \hat{\mathbf{p}}_s \sin(\mathbf{p} \cdot \mathbf{R}), \quad (44)$$

where $\hat{\mathbf{p}}_s = (1 + \nu)^{-1/2}(1, -\sqrt{\nu})$ is the vector $\hat{\mathbf{p}}$ mirror reflected about the x -axis. With $\hat{\mathbf{p}}$ close to the diagonal, the displacement field is predominantly shear-type (and a perfect shear distortion in the incompressible limit $\kappa \rightarrow \infty$). Finally, the displacement (44) relaxes the energy of the hexagonal lattice to

$$g_{\text{dh}}(V) = g_\Delta(V) - \frac{nV^2}{64s^2\mu} (1 + \mu/\kappa). \quad (45)$$

Note that the displacement \mathbf{u} diverges $\propto s^{-2}$ on approaching the density $n = \sqrt{3}/2b^2$ where $h = b$ and $s = 0$ and our approximation breaks down. Limiting the displacement u to a fraction $c \sim 0.1$ of the lattice constant a then restricts the validity of our analysis to potentials $V < 8\pi\sqrt{1+\nu}c(\mu/n)s^2$. Higher order (in V) corrections are of order V^4 in the energy relaxation g_{dh} and of order V^2 in the angle φ_{\min} . Rather than studying such corrections in V , we proceed with the analysis of the full non-linearity in the force field which takes us to a non-uniform soliton phase. The precision of this calculation then is limited by our use of the harmonic approximation (to be improved later with a numerical analysis) and the resonance approximation (to be abandoned when including the second mode of the substrate potential in Sec. VII).

V. SOLITON PHASE IN THE RESONANCE APPROXIMATION

With increasing V , the periodic shear-type displacement (44) evolving along the misfit vector \mathbf{p} becomes large, of order b , and turns into a soliton array as first described by Pokrovsky and Talapov^{19,20} within the resonance approximation discussed above. For completeness, we will briefly sketch their analysis and present the main

results here. We describe the change in the interaction energy within the harmonic approximation, adopting the long wave-length approximation, introduced in Sec. III and used in Sec. IV, in a continuum elastic formulation [$\mathbf{R}_i^\Delta \rightarrow \mathbf{R}$, $\mathbf{u}_i \rightarrow \mathbf{u}(\mathbf{R})$, see also appendix C 1],

$$\delta g_\Delta^{\text{int}} = \frac{1}{N} \int_A d^2 R \left[\frac{\kappa}{2} (\partial_x u_x + \partial_y u_y)^2 + \frac{\mu}{2} ((\partial_x u_x - \partial_y u_y)^2 + (\partial_y u_x + \partial_x u_y)^2) \right]. \quad (46)$$

The drive in the substrate potential derives from the misfit between the lattice positions \mathbf{R}_i^Δ and the \mathbf{q} -vector; this can be made more explicit by the transformation $\mathbf{q} \cdot \mathbf{R}_i^\Delta \rightarrow (\mathbf{K} - \mathbf{p}) \cdot \mathbf{R}_i^\Delta = -\mathbf{p} \cdot \mathbf{R}_i^\Delta + 2\pi\mathbb{Z}$. Within the continuum approximation, the substrate potential contributes with a term (we use $\mathbf{q} \cdot (\mathbf{R} + \mathbf{u}) = -\mathbf{p} \cdot \mathbf{R} + \mathbf{q} \cdot \mathbf{u}$)

$$e^{\text{sub}} = \frac{1}{N} \int_A d^2 R \frac{nV}{2} [2 - \cos(\mathbf{p} \cdot \mathbf{R} - \mathbf{q} \cdot \mathbf{u})], \quad (47)$$

where we account for the additional average energy $V/2$ of the second mode. The task then is to minimize the total free energy $g(V) = g_\Delta(V) + \delta g_\Delta^{\text{int}} + e^{\text{sub}}$. For small amplitudes V this is achieved by the period modulation $\mathbf{u}(\mathbf{R})$ in (44) of the φ -rotated hexagonal lattice. At large values of V , the lowest energy will be assumed by a rhombic or isosceles triangular lattice with height b (along x) and base b' (along y), the so-called bb' rhombic lattice (within the resonance approximation, we account only for the leading substrate mode that we choose along x). In order to find this lattice, we minimize the free energy $g(V)$ at large V with respect to a global displacement field

$$\mathbf{u}_g(\mathbf{R}) = \begin{pmatrix} \mathbf{w} \cdot \mathbf{R} \\ \mathbf{t} \cdot \mathbf{R} \end{pmatrix}, \quad (48)$$

parametrized by the vectors $\mathbf{w} = (w_1, w_2)$ and $\mathbf{t} = (t_1, t_2)$. Minimizing $\delta g_\Delta^{\text{int}}[\mathbf{u}_g] = (\kappa/2n)(w_1 + t_2)^2 + (\mu/2n)(w_2 + t_1)^2$ with respect to \mathbf{t} at fixed \mathbf{w} , we find that $t_1 = -w_2$ and $t_2 = -\nu w_1$, resulting in a displacement

$$\mathbf{u}_g(\mathbf{R}) = w_1 \begin{pmatrix} x \\ -\nu y \end{pmatrix} - w_2 \begin{pmatrix} -y \\ x \end{pmatrix} = \mathbf{u}_d + \mathbf{u}_r \quad (49)$$

that combines a shear displacement \mathbf{u}_d (a stretching by w_1 along x and a compression by $w_1\nu$ along y) and a rotation \mathbf{u}_r (by the angle $-w_2$; note that we cannot go beyond the linearized rotation \mathbf{u}_r as higher order terms are beyond our accuracy and generate unphysical terms). At large V , the potential minima lock the particles into a rhombic lattice with height b along x , hence $(1+w_1)h = b$ and $w_1 = s$; at the same time, the rotation has to align the particle lattice back to the substrate, hence $w_2 = \varphi = s\sqrt{\nu}$ (here we drop the index and rename $\varphi = \varphi_{\text{min}}$), hence $\mathbf{w} = s(1, \sqrt{\nu})$. The global displacement field (49) then can be written in the form [we define the coordinate $z = (x + \sqrt{\nu}y)/\sqrt{1+\nu}$]

$$\mathbf{u}_g = s\sqrt{1+\nu} z \begin{pmatrix} 1 \\ -\sqrt{\nu} \end{pmatrix} \quad (50)$$

and generates the new bb' rhombic lattice out of the hexagonal one. The lattice constant b' along the y -axis assumes a value intermediate between b and a ,

$$b' = a(1 - \nu s) \approx 1.0090 b > b. \quad (51)$$

The elastic energy required to generate this distortion is

$$\delta g_\Delta^{\text{int}} = g_{\triangleright'} - g_\Delta \approx \frac{\kappa}{\kappa + \mu} \frac{2\mu}{n} s^2 = 0.0169 e_D. \quad (52)$$

Note that this deformation involves a change in density or area $\delta A/A = \nabla \cdot \mathbf{u}_d = s(1 - \nu) = 0.0136$. A more accurate result is obtained by minimizing the free energy $g_{\triangleright'}(b') = e_{\triangleright'}^{\text{int}}(b') + p/n'$ with respect to b' , fixing the height of the rhombic lattice to b ; here, $e_{\triangleright'}^{\text{int}}$ is the true interaction energy in Eq. (1) (to be calculated with the Ewald technique) and $n' = 1/bb'$. The result of such a calculation provides the base length $b' \approx 1.0173 b$ and $g_{\triangleright'} - g_\Delta = 0.0179 e_D$. The relative difference $(b - b')/(a - b) \approx 0.11$ is quite large, of the order of 10 %, indicating that the result of the elastic theory is not very accurate.

Next, we determine the non-uniform soliton phase that interpolates between the rotated distorted hexagonal lattice at small substrate potential V and the bb' rhombic lattice at large V . We adopt an Ansatz $\mathbf{u} = \mathbf{u}'_g + \tilde{\mathbf{u}}$ for the displacement field involving a periodic modulation $\tilde{\mathbf{u}}$ on top of a global displacement \mathbf{u}'_g (parametrized by \mathbf{w}' and \mathbf{t}'). The parameters \mathbf{w}' , \mathbf{t}' now depend on the amplitude V of the substrate potential with $\mathbf{w}' = 0$ at $V = 0$ and $\mathbf{w}' = \mathbf{w}$ at large V . Inserting this Ansatz into the free energy $g = g_\Delta + \delta g_\Delta + e^{\text{sub}}$, we first minimize with respect to \mathbf{t}' to find that $\mathbf{t}' = -(w'_2, \nu w'_1)$. The free energy per particle then assumes the form

$$g = g_{\text{bg}}(V) + \frac{1}{N} \int_A d^2 R \left\{ \frac{\kappa}{2} (\partial_x \tilde{u}_x + \partial_y \tilde{u}_y)^2 + \frac{\mu}{2} [(\partial_x \tilde{u}_x - \partial_y \tilde{u}_y)^2 + (\partial_y \tilde{u}_x + \partial_x \tilde{u}_y)^2] + \frac{nV}{2} [1 - \cos(\mathbf{p}' \cdot \mathbf{R} - q\tilde{u}_x)] \right\}. \quad (53)$$

with $g_{\text{bg}}(V) = g_\Delta + [2\mu\kappa/n(\kappa + \mu)](s - s')^2 + V/2$ the energy of the homogeneous background and

$$\mathbf{p}' = \mathbf{p} - q\mathbf{w}' \equiv q \begin{pmatrix} s' \\ \varphi' \end{pmatrix}. \quad (54)$$

The further minimization of (53) with respect to the periodic displacement $\tilde{\mathbf{u}}$ and the effective misfit vector $\mathbf{p}'(V)$, see Fig. 10, will provide us with the geometry of the non-uniform soliton phase. The misfit vector \mathbf{p}' starts out with $\mathbf{p} = qs(1, \sqrt{\nu})$ at $V = 0$, see Eq. (42), and vanishes in the bb' rhombic phase at large V where $\mathbf{w}' = \mathbf{w} = s(1, \sqrt{\nu})$; the parameters s' and φ' describe the evolution of the global displacement as a function of V .

Minimizing (53) with respect to the periodic displacement field $\tilde{\mathbf{u}}$, we obtain the set of differential equations

$$\begin{aligned} \kappa(\partial_x^2 \tilde{u}_x + \partial_x \partial_y \tilde{u}_y) + \mu \Delta \tilde{u}_x &= \frac{-nV}{2} q \sin(\mathbf{p}' \cdot \mathbf{R} - q\tilde{u}_x), \\ \kappa(\partial_x \partial_y \tilde{u}_x + \partial_y^2 \tilde{u}_y) + \mu \Delta \tilde{u}_y &= 0. \end{aligned} \quad (55)$$

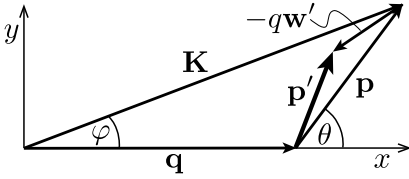


FIG. 10: The effective mismatch \mathbf{p}' is a combination of the true mismatch \mathbf{p} and the correction $-\mathbf{q}\mathbf{w}'$ due to the global displacement field \mathbf{u}'_g .

These equations admit a uniaxial solution $\tilde{\mathbf{u}}(x, y) = \tilde{\mathbf{u}}(z')$ along $z' = x \cos \theta' + y \sin \theta'$ with the direction of z' determined by the effective mismatch vector $\mathbf{p}' = p'(\cos \theta', \sin \theta')$ and the boundary condition $\tilde{\mathbf{u}}(z') = \tilde{\mathbf{u}}(z' + L)$ with $L = 2\pi/p'$. The second equation relates the two components of the displacement field via

$$\tilde{u}_y = -\eta(\theta') \tilde{u}_x \quad \text{with} \quad \eta = \frac{\kappa \sin \theta' \cos \theta'}{\kappa \sin^2 \theta' + \mu}, \quad (56)$$

where we have used the boundary condition $\tilde{u}_x(0) = \tilde{u}_x(L) = 0$ and the same for \tilde{u}_y . Assuming $\kappa \gg \mu$, η increases with θ' from zero, $\eta \approx (\kappa/\mu)\theta'$, goes through a maximum $\eta \approx \sqrt{\kappa/\mu}/2$ at $\theta' \approx \sqrt{\mu/\kappa}$, decreases as $\eta \approx \cot \theta'$, and approaches zero at $\pi/2$ linearly as $\eta \approx (1 - \mu/\kappa)(\pi/2 - \theta')$; while for angles close to 0 and $\pi/2$, the y -component \tilde{u}_y is very small, it increases to about 1.5 times the x -component \tilde{u}_x for $\kappa/\mu = 10$.

Inserting the result (56) back into the first equation of (55) and transforming variables $\tilde{z} = \mathbf{p}' \cdot \mathbf{R} = p'z'$, $u = \tilde{z} - q\tilde{u}_x$, we obtain the Sine-Gordon equation

$$\tilde{\alpha} \partial_{\tilde{z}}^2 u = \sin u, \quad (57)$$

with boundary conditions $u(0) = 0$ and $u(2\pi) = 2\pi$ and

$$\tilde{\alpha} = \frac{2\mu}{Vn} \frac{\kappa + \mu}{\kappa \sin^2 \theta' + \mu} \left(\frac{p'}{q} \right)^2. \quad (58)$$

With the total displacement $qu_x = (\mathbf{p} \cdot \mathbf{R} - \tilde{z}) + q\tilde{u}_x$, the displacement $u = \tilde{z} - q\tilde{u}_x$ contributes both to the global and periodic parts of u_x . Indeed, u has a stair-case shape, while the periodic function $q\tilde{u}_x$ has a saw-tooth form.

In the limit $p' \rightarrow 0$ we have $L \rightarrow \infty$ and it is convenient to rewrite (57) in the form $\alpha \partial_{z'}^2 u = \sin u$ with $\alpha = \tilde{\alpha}/p'^2$ and boundary conditions $u(-\infty) = 0$ and $u(\infty) = 2\pi$. The single-soliton solution then is given by

$$u(z') = 4 \arctan[\exp(z'/\sqrt{\alpha})], \quad (59)$$

with a core region of width $\sqrt{\alpha} \approx (b/2\pi \sin \theta') \sqrt{2\mu/Vn}$, where we have dropped the correction from the shear modulus μ in α . Within this core region, $\tilde{u}_x = -u/q$ quickly goes from 0 to $-b$.

At finite p' , the solution is given by a soliton array with period $L = 2\pi/p'$ as obtained by integrating the ‘velocity’ $\partial_{z'} u = [2(\tilde{\alpha}_0 - \cos u)/\tilde{\alpha}]^{1/2}$, with the integration constant $\tilde{\alpha}_0$ (the minimal slope between subsequent

solitons) given by the implicit equation (K is the complete elliptic integral of the first kind³²)

$$(\pi/2) \sqrt{2(1 + \tilde{\alpha}_0)/\tilde{\alpha}} = K[\sqrt{2/(1 + \tilde{\alpha}_0)}] \quad (60)$$

and assuming asymptotic values $\tilde{\alpha}_0(\tilde{\alpha} \rightarrow 0) \rightarrow 1$ (single sharp soliton at large V or small misfit p') and $\tilde{\alpha}_0(\tilde{\alpha} \rightarrow \infty) \rightarrow \tilde{\alpha}/2$ (smoothly modulated and steadily increasing solution $u \approx \tilde{z}$ at small V as solitons strongly overlap).

In order to find the parameter p' (the soliton density $1/L = p'/2\pi$) and the angle θ' of the soliton array, we have to minimize the energy (53) of the solitonic solution. After the reduction to a one-dimensional Sine-Gordon problem, we find the expression

$$g - g_{\text{bg}} = \frac{V}{2} \int_0^{2\pi} \frac{d\tilde{z}}{2\pi} \left[\frac{\tilde{\alpha}}{2} (\partial_{\tilde{z}} u - 1)^2 + 1 - \cos u \right] \quad (61)$$

$$= \frac{V}{2} (1 - \tilde{\alpha}_0 - \tilde{\alpha}/2) + \frac{V}{\pi} \sqrt{2\tilde{\alpha}(1 + \tilde{\alpha}_0)} E[\sqrt{2/(1 + \tilde{\alpha}_0)}]$$

with E the complete elliptic integral of the second kind, see Ref. 32. The energy Eq. (61) grows monotonically with $\tilde{\alpha}$, starting from 0 at $\tilde{\alpha} = 0$ (large V) and saturating at $V/2$ as $\tilde{\alpha} \rightarrow \infty$ (small V). Expressing $\tilde{\alpha}$ through s' and φ' , see Eqs. (54) and (58), we minimize $\tilde{\alpha}$ with respect to φ' (note that φ' only enters the soliton energy, while s' also appears in g_{bg}) and obtain the minimal value

$$\tilde{\alpha} = \frac{2\mu}{Vn} \frac{4\kappa}{\kappa + \mu} s'^2 \quad \text{at} \quad \varphi' = \sqrt{\nu} s' \quad (62)$$

and hence the direction of the (effective) misfit \mathbf{p}' coincides with that of \mathbf{p} in Eq. (42),

$$\mathbf{p}' = qs' \begin{pmatrix} 1 \\ \sqrt{\nu} \end{pmatrix} \quad \text{and} \quad \theta' = \theta = \arctan \sqrt{\nu}, \quad (63)$$

i.e., the dense soliton array smoothly appears out of the perturbative displacement modulation (44) of the locked phase found in Sec. IV. The soliton density is given by $1/L = s'\sqrt{1 + \nu}/b$ and the global displacement field in Eq. (49) which takes the hexagonal phase smoothly into the bb' rhombic lattice reads

$$\mathbf{u}'_g(\mathbf{R}) = (s - s')\sqrt{1 + \nu} z \begin{pmatrix} 1 \\ -\sqrt{\nu} \end{pmatrix}, \quad (64)$$

where we have used that $\mathbf{w}' = (s - s')(1, \sqrt{\nu})$ and $\sqrt{1 + \nu} z = x + \sqrt{\nu} y$, see Eq. (63). At small V , $s' = s$, the density of solitons is high, $\mathbf{u}'_g = 0$, and the lattice is close to the hexagonal one. For a large substrate potential V , $s' = 0$, the density of solitons vanishes, $\mathbf{u}'_g = \mathbf{u}_g$, and the particles are arranged in the bb' rhombic lattice. An alternative—and actually the conventional—view is to start from the bb' rhombic lattice at large V , the commensurate phase, and then have solitons deform the lattice until the dense soliton array describes the hexagonal phase. The shape of the individual soliton (along x) is given by Eq. (59) and making use of the result (63) for the angle θ and Eq. (56), we find the

ratio $\eta = \sqrt{\nu}$, i.e., the displacement field of one soliton is $\mathbf{d}^{\text{PT}} = b(-1, \sqrt{\nu}) \approx b(1, -0.905)$. As the solitons become denser with decreasing V , their shift vectors add up to produce the global displacement field $\mathbf{u}'_{\text{g}} - \mathbf{u}_{\text{g}}$ on top of the rhombic lattice until the latter has transformed into the hexagonal lattice at vanishing V (where $\mathbf{u}'_{\text{g}} = 0$). The periodic part $\tilde{\mathbf{u}}$ of the displacement field coincides with the result (44) of the perturbative analysis at small V and turns into a saw-tooth shape with sharp shifts $\sim b(-1, \sqrt{\nu})$ in the core regions and a small slope $\tilde{\mathbf{u}} \approx (\mathbf{p}' \cdot \mathbf{R}/q)(1, -\sqrt{\nu})$ in between two solitons.

It remains to calculate the critical substrate potential V_c^{PT} for the first soliton entry on decreasing V and the dependence $s'(V)$ determining the density $1/L$ of solitons. This last step involves the minimization of $g(s'; V)$ with respect to s' at fixed V .

At small V , where $\tilde{\alpha}$ is large, we set $\tilde{\alpha}_0 \approx \tilde{\alpha}/2$ and expand the energy (61) to order $1/\tilde{\alpha}$,

$$g \approx g_{\Delta} + V + \frac{\kappa}{\kappa + \mu} \frac{2\mu}{n} (s - s')^2 - \frac{nV^2}{64s'^2\mu} (1 + \mu/\kappa). \quad (65)$$

The optimal s' then satisfies the equation $\partial_{s'} g = 0$, i.e.,

$$(s - s') \approx \frac{n^2 V^2 (1 + \mu/\kappa)^2}{128\mu^2 s'^3} \quad (66)$$

and we find that $(s - s') \propto V^2$. Hence, we can set $s = s'$ in Eq. (65) and the free energy assumes the form

$$g \approx g_{\Delta}(V) - \frac{nV^2}{64s'^2\mu} (1 + \mu/\kappa) \quad (67)$$

in agreement with the Eq. (45). Furthermore, the angle $\varphi' \approx \varphi$ up to corrections of order V^2 .

At large values of V , we can approximate the complete elliptic integrals³³ K and E to arrive at the free energy in the form

$$g \approx g_{\Delta} + \frac{V}{2} + \frac{\gamma}{2} s^2 + (\epsilon - \gamma s) s' + 4\epsilon s' e^{-4V/\epsilon s'}, \quad (68)$$

where we have defined the elastic and soliton energies

$$\gamma = \frac{\kappa}{\kappa + \mu} \frac{4\mu}{n}, \quad \epsilon = \frac{4}{\pi} \sqrt{\frac{\kappa}{\kappa + \mu} \frac{V}{2} \frac{4\mu}{n}}. \quad (69)$$

The first three terms of Eq. (68) represent the energy $g_{\triangleright'}$ of the bb' rhombic structure. The term $(\epsilon - \gamma s)s'$ turns negative when the soliton energy ϵ is balanced against the drive (or chemical potential for solitons) γs . Finally, the last term describes the exponential interaction between solitons and stabilizes s' at a finite value, i.e., a finite soliton density. The transition from the bb' rhombic phase to the non-uniform soliton phase then takes place when $\epsilon = \gamma s$, corresponding to the critical substrate strength

$$V_c^{\text{PT}} = \frac{\pi^2}{2} \frac{\kappa}{\kappa + \mu} \frac{\mu}{n} s^2. \quad (70)$$

For particles interacting via a $1/r^3$ -potential, the compression and shear moduli fulfill the relation $\kappa = 10\mu$, see Eq. (13), such that at commensurate density one finds the critical substrate amplitude³⁴

$$V_c^{\text{PT}} = \frac{5\pi^2}{11} \frac{\mu}{n} s^2 = 0.0416 e_D \quad \text{at } \theta = 42.13^\circ. \quad (71)$$

We find the effective misfit parameter $s'(V)$ by minimizing the free energy (68), $\partial_{s'} g = 0$, providing us with the relation

$$(\epsilon - \gamma s) + 4\epsilon e^{-4V/\epsilon s'} (1 + 4V/\epsilon s') = 0. \quad (72)$$

The last factor is dominated by the term $4V/\epsilon s'$. Close to V_c^{PT} , we write $V = V_c^{\text{PT}}(1 - \delta)$ with $0 < \delta \ll 1$ and find

$$s' \approx -\frac{4V_c^{\text{PT}}}{\gamma s} \frac{1}{\log(\delta/8)} = \frac{\pi^2}{2|\log[(1 - V/V_c^{\text{PT}})/8]|} s, \quad (73)$$

where we have used that $\epsilon_c = \gamma s$ in the last step. Combining Eqs. (68) and (73), we obtain the free energy near the transition

$$g = g_{\Delta} + \frac{V}{2} + \frac{\kappa}{\kappa + \mu} \frac{2\mu}{n} s^2 - \frac{2(V_c^{\text{PT}} - V)}{\log[8V_c^{\text{PT}}/(V_c^{\text{PT}} - V)]}. \quad (74)$$

Hence, we find that decreasing V below V_c^{PT} , the particle system is rapidly flooded with solitons, $n_{\text{sol}} \propto 1/|\log[(1 - V/V_c^{\text{PT}})]|$, similar to the rapid entry of flux lines in a type II superconductor when the field H is increased above the lower critical fields H_{c1} . This result, is changed to an algebraic behavior $n_{\text{sol}} \propto \sqrt{1 - V/V_c^{\text{PT}}}$ for V very close to V_c^{PT} , a consequence of the long-range interaction $\propto 1/R^3$ between particles. The latter generates an algebraic repulsion $\propto (b/L)^2$ between solitons, see Eq. (118) below, replacing the exponential law $\propto \exp[-\pi(L/b)\sqrt{Vn/\mu}]$ in Eq. (68) at large distances³⁵.

VI. SOLITONS WITH ONE SUBSTRATE MODE

Having understood the appearance and evolution of the non-uniform soliton phase in the 2D hexagonal particle system with increasing substrate potential V , we now focus on the first appearance of the (PT or Pokrovsky-Talapov) soliton when decreasing the substrate potential V in the bb' rhombic phase. Using the elastic theory of the hexagonal lattice, we expect to find accurate results for the distorted hexagonal phase and the dense vortex array at small substrate potential V . On the other hand, the first PT soliton appears out of the commensurate phase at large substrate amplitudes V and accordingly, we expect more accurate results for V_c^{PT} when using the elastic theory for the bb' -lattice. Furthermore, the comparison of the results provided by these different starting points will tell us about the relevance of anharmonicities and guide us when evaluating the critical potentials V_c for the first soliton entry in the presence of both lattice

modes, see Sec. VII. We first find an analytical result based on elasticity theory and then compare with numerical results using direct summation of the interaction and substrate potential energies in (1).

A. Continuum elastic approach

We define the displacement field $\mathbf{v}(\mathbf{R})$ with respect to the rhombic lattice $\mathbf{R}_{m,n}^{\triangleright} = (mb, (n-m/2)b') \equiv \mathbf{R}$ and assume a uniaxial defect $\mathbf{v}(z)$ evolving along z , shifting the lattice by $\mathbf{v}(\infty) = (-b, v_{y,\infty})$ with $v_{y,\infty}$ to be determined (the soliton starts at $\mathbf{v}(-\infty) = (0,0)$). We then have to minimize the soliton line energy

$$\varepsilon = \int_{-\infty}^{\infty} dz \left\{ g_{\triangleright}^{\text{el}}(\mathbf{v}) + \frac{n'V}{2} [1 - \cos(-qv_x)] \right\} \quad (75)$$

with the rhombic lattice density $n' = 1/bb'$. Furthermore, we have used that $\mathbf{q} \cdot \mathbf{R} = 2\pi\mathbb{Z}$ as the undisturbed bb' lattice is in registry with the substrate potential along the x -axis. The above soliton line energy relates to the usual free energy density via

$$\varepsilon \approx \lim_{L, L_{\perp} \rightarrow \infty} L_{\perp}^{-1} \int_{L \times L_{\perp}} dz dz_{\perp} [g_{\triangleright}^{\text{el}}(\mathbf{v}) + n' e^{\text{sub}}(\mathbf{R} + \mathbf{v})]. \quad (76)$$

The elastic theory of the bb' -lattice is described by the energy density $g_{\triangleright}^{\text{el}} = g_p + g_{\kappa} + g_{\mu}$ with the linear term

$$g_p = (\gamma'_x + p)(\partial_x v_x) + (\gamma'_y + p)(\partial_y v_y) \quad (77)$$

driving the system towards the hexagonal phase and the usual compression- and shear-type energy densities

$$g_{\kappa} = \frac{\kappa'_x}{2} (\partial_x v_x)^2 + \frac{\kappa'_y}{2} (\partial_y v_y)^2 + \kappa'_{xy} (\partial_x v_x)(\partial_y v_y), \quad (78)$$

$$g_{\mu} = \frac{\mu'_x}{2} (\partial_y v_x)^2 + \frac{\mu'_y}{2} (\partial_x v_y)^2 + \mu'_{xy} (\partial_y v_x)(\partial_x v_y).$$

The linear contribution (77) is due to the purely repulsive dipolar interaction that is balanced only by the external pressure term $p\delta A/A$ and has been included in $g_{\triangleright}^{\text{el}}$; for the hexagonal lattice this pressure term generates a stable minimum relating to the density via Eq. (5) and balances the γ terms, $\gamma_x = \gamma_y = -p$. Deforming the hexagonal lattice into the bb' rhombic lattice (in our case via the underlying substrate potential) this term attempts to drive the particle lattice back to the rhombic shape as the γ' -terms are not compensated by the pressure. The various coefficients $\gamma'_{x,y}$, $\kappa'_{x,y,xy}$, and $\mu'_{x,y,xy}$ are determined with the help of the Ewald summation technique²⁴ as described in the appendix C.

Assuming a uniaxial soliton $\mathbf{v}(z)$ oriented along $z = x \cos \theta + y \sin \theta$ (with θ to be determined), the expression for the total line energy (76) can be simplified and naturally splits into a soliton part

$$\varepsilon_s = \int_{-\infty}^{\infty} dz \left\{ \frac{\kappa'_x \cos^2 \theta + \mu'_x \sin^2 \theta}{2} (\partial_z v_x)^2 + \frac{\kappa'_y \sin^2 \theta + \mu'_y \cos^2 \theta}{2} (\partial_z v_y)^2 \right. \\ \left. + (\kappa'_{xy} + \mu'_{xy}) \sin \theta \cos \theta (\partial_z v_x)(\partial_z v_y) + \frac{Vn'}{2} [1 - \cos(-qv_x)] \right\} \quad (79)$$

and a drive

$$\varepsilon_d = \int_{-\infty}^{\infty} dz (\gamma'_x + p) \cos \theta (\partial_z v_x) = -(\gamma'_x + p) b \cos \theta, \quad (80)$$

where we have used the boundary condition $v_x(\infty) = -b$. Minimizing the soliton energy, we obtain a Sine-Gordon equation $\alpha_{\triangleright} \partial_z^2 (qv_x) = \sin(qv_x)$ with

$$\alpha_{\triangleright} = \frac{2}{Vn'q^2} \left[\kappa'_x \cos^2 \theta + \mu'_x \sin^2 \theta - \frac{(\kappa'_{xy} + \mu'_{xy})^2 \cos^2 \theta}{\kappa'_y + \mu'_y \cot^2 \theta} \right]. \quad (81)$$

The displacement v_y along y is slaved to the displacement along x via $v_y = -\eta_{\triangleright} v_x$ with

$$\eta_{\triangleright} = \frac{(\kappa'_{xy} + \mu'_{xy}) \cot \theta}{\kappa'_y + \mu'_y \cot^2 \theta} \quad (82)$$

and the soliton line energy takes the form

$$\varepsilon_s = 4n'V \sqrt{\alpha_{\triangleright}}. \quad (83)$$

The first soliton appears when the soliton and drive energies compensate one another, $\varepsilon = \varepsilon_s + \varepsilon_d = 0$; figure 11 shows these energies as a function of angle θ at the critical potential where the minimum in ε vanishes for the first time, providing the critical substrate potential and the soliton angle

$$V_c^{\text{PT}} = 0.0417 e_D, \quad \theta = 45.05^\circ. \quad (84)$$

The lattice displacement along y associated with this soliton is determined by $\eta_{\triangleright} \approx 0.696$ and we obtain the overall shift vector for the Pokrovskii-Talapov soliton $\mathbf{d}^{\text{PT}} = b(-1, 0.696)$.

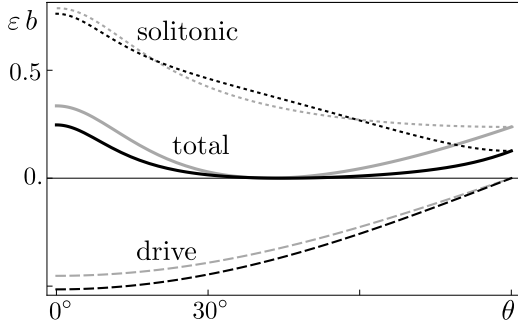


FIG. 11: Solitonic energy $\varepsilon_s b$ (dotted) and drive $\varepsilon_d b$ (dashed) calculated with the elastic theory for the rhombic lattice (black) and the one for the hexagonal lattice (grey) at the critical potential $V_c^{\text{PT}} \approx 0.0417 e_D$ in units of e_D . The solid lines represent the total energy $\varepsilon b = \varepsilon_d b + \varepsilon_s b$.

At first sight, these results compare favorably with those obtained using the elasticity theory for the hexagonal lattice, particularly for the critical potential V_c^{PT} , see Eqs. (71) and (84), and to a lesser degree for θ ; the results for the shift along y differ quite substantially, however, $\eta \approx 0.905$ versus $\eta_{\triangleright'} \approx 0.696$. Furthermore, Fig. 11 shows, that the individual results for the soliton energy ε_s and the drive ε_d again differ quite appreciably. Overall, we have to conclude that anharmonicities are not negligible and have the potential to change the results on the order of 10 %.

B. Numerical analysis

In order to obtain accurate and reliable results for the first appearance (at V_c^{PT}) and the characteristic parameters (θ, η) of the PT soliton, we determine these quantities with the help of a numerical analysis. Such an analysis will be even more relevant when analyzing solitons and domain walls in the presence of two substrate modes, see Sec. VII below. In the following, we determine the optimal shape for the PT soliton within a variational approach and find the critical substrate potential V_c^{PT} . The latter is determined by comparing the free energies with and without soliton on the bb' -lattice background as calculated directly from the ‘microscopic’ expressions Eqs. (1) and (3), where the geometry of the bb' -lattice is determined by minimization of $g_{\triangleright'}(b')$ with $b' = 1.0173 b$.

Summing the long-range interaction for a two-dimensional particle system is unpractical (note that the Ewald summation cannot be applied to the non-uniform soliton phase). However, we can reduce the problem to a one-dimensional one by selecting angles θ where z_{\perp} is directed along a particle row, see Fig. 12. We then make use of appropriate supercells with lattice vectors arranged along the z_{\perp} -axis and along the y -axis, $\mathbf{a}_1 = (mb, -nb')$ and $\mathbf{a}_2 = (0, b')$ where m and n are Miller indices. Below, we analyze configurations with small Miller indices,

$m = n = 2$ with $\theta = \arctan(mb/nb') = 44.5^\circ$ and 2 particles per supercell, $m = 2, n = 1$ with $\theta = 63.4^\circ$, $m = 2, n = 3$ with $\theta = 33.2^\circ$, and $m = 2, n = 5$ with $\theta = 21.5^\circ$ and 1 particle per cell, and $m = 4, n = 1$ with $\theta = 75.7^\circ$ and 4 particles per supercell. The matrix

$$U_{m,n} = \frac{1}{a_1} \begin{pmatrix} mb & -nb' \\ nb' & mb \end{pmatrix} \quad (85)$$

transforms the coordinates from the xy - to the $z_{\perp}z$ -frame, in particular, $\mathbf{a}_1 = (a_1, 0)$ and $\mathbf{a}_2 = (-nb'^2/a_1, mbb'/a_1)$. In the following, we sketch the main steps of the analysis for the case $m = n = 2$, see Fig. 12, and cite the results for the remaining cases.

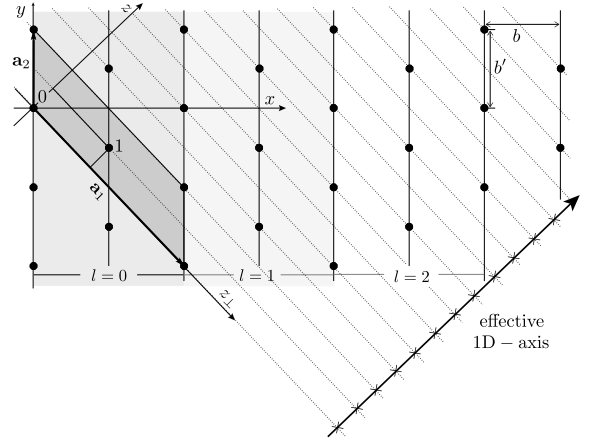


FIG. 12: Coordinates z_{\perp} and z for $m = n = 2$, $\theta \approx 44.5^\circ$ with a supercell containing two particles with labels 0 and 1.

The sums in the energy $E(A, N)$, Eq. (1), involve the particle positions of the bb' lattice

$$\mathbf{R}_{lq}^{\triangleright', \mu} = \begin{pmatrix} z_{\perp, lq}^{\mu} \\ z_q^{\mu} \end{pmatrix} = l\mathbf{a}_1 + q\mathbf{a}_2 + U_{2,2}\mathbf{c}^{\mu}, \quad (86)$$

with the basis $\mathbf{c}^0 = (0, 0)$ and $\mathbf{c}^1 = (b, -b'/2)$ (in the xy -frame) and the positions of the distorted lattice including one soliton

$$\mathbf{R}_{lq}^{s, \mu} = \begin{pmatrix} z_{\perp, lq}^{s, \mu} \\ z_q^{s, \mu} \end{pmatrix} = \mathbf{R}_{lq}^{\triangleright', \mu} + U_{2,2} \begin{pmatrix} v_x(z_q^{\mu}) \\ v_y(z_q^{\mu}) \end{pmatrix}, \quad (87)$$

with the soliton displacement field (again in the xy -frame)

$$v_x(z) = -\frac{2b}{\pi} \arctan\{\exp[(z - z_s)/\sqrt{w_x\alpha}]\}, \quad (88)$$

$$v_y(z) = s_y \eta \frac{2b}{\pi} \arctan\{\exp[(z - z_s)/\sqrt{w_y\alpha}]\}. \quad (89)$$

Here, z_s defines the soliton position and w_x, w_y , and s_y are variational parameters for the soliton widths (along x and y) and the soliton shift along y with respect to the

values for α (see (81)) and η (see (82)) obtained from the analytic results based on the bb' rhombic lattice.

A fast evaluation of the interaction energy in $E(A, N)$ is crucial for the optimization process of the soliton shape and the evaluation of V_c^{PT} . The sum

$$E_s^{\text{int}} = \frac{1}{2} \sum_{l, l', q, q', \mu, \nu} \frac{D}{|\mathbf{R}_{lq}^{s, \mu} - \mathbf{R}_{l'q'}^{s, \nu}|^3} \quad (90)$$

is split into one along z_{\perp} (over l and l') which can be resummed analytically and the remaining sum along z (over q and q'). Using Poisson's formula at fixed shifts $\alpha = \alpha_{qq'}^{s, \mu\nu} = (z_{\perp, 0q}^{s, \mu} - z_{\perp, 0q'}^{s, \nu})/a_1$ along z_{\perp} in the supercell $l = 0$ and $\beta = \beta_{qq'}^{s, \mu\nu} = (z_q^{s, \mu} - z_{q'}^{s, \nu})/a_1$ along z , we find that (see also appendix B)

$$\begin{aligned} \sum_l \frac{1}{[(l + \alpha)^2 + \beta^2]^{3/2}} & \quad (91) \\ &= \frac{2}{\beta^2} + 8\pi \sum_{\bar{l} > 0} \bar{l} \cos(2\pi\bar{l}\alpha) \frac{K_1(2\pi\bar{l}|\beta|)}{|\beta|} \end{aligned}$$

can be approximated by taking only few terms (of order 10) in the second sum over \bar{l} , as the modified Bessel function $K_1(z)$ (of the second kind) rapidly decreases, $K_1(z) \propto e^{-z}$ for large z (see Ref. 32). The remaining sums in the interaction energy

$$\begin{aligned} E_s^{\text{int}} &= \frac{N_{\perp} D}{2a_1^3} \sum_{q, q', \mu, \nu} \left\{ \frac{2}{(\beta_{qq'}^{s, \mu\nu})^2} \right. \\ &\quad \left. + 8\pi \sum_{\bar{l} > 0} \bar{l} \cos(2\pi\bar{l}\alpha_{qq'}^{s, \mu\nu}) \frac{K_1(|2\pi\bar{l}\beta_{qq'}^{s, \mu\nu}|)}{|\beta_{qq'}^{s, \mu\nu}|} \right\} \quad (92) \end{aligned}$$

then have to be evaluated numerically. Here, N_{\perp} denotes the number of unit cells (of extension $a_1 = 2\sqrt{b^2 + b'^2}$) along z_{\perp} . The sums are to be taken over the particles $\mu, \nu \in \{0, 1\}$ in the supercell and $q, q' \in \{0, \dots, N/2 - 1\}$ go over the supercells in the $l = 0$ strip, see Fig. 12, with N the particle number in the $l = 0$ strip. Equation (92) then evaluates the interaction energy of a one-dimensional chain of particles with an effective interaction that accounts for the transverse dimension. Note that the terms with $q = q'$ at $\mu = \nu$ are discarded as these are compensated by an equal term appearing in the interaction energy E_{int} without the soliton (the two compensating terms are easily evaluated via the direct sum $(D/2) \sum_{l \neq 0} (a_1 l)^{-3} = D\zeta(3)/2a_1^3$ with $\zeta(s) = \sum_{n=1}^{\infty} n^{-s}$ the Riemann zeta function).

The substrate energy E_s^{sub} in Eq. (1) is cast into a similar form with the sum going over all basis vectors $\mu \in \{0, 1\}$ in the supercell and summation over cells $q \in \{0, \dots, N/2 - 1\}$ in the $l = 0$ -strip,

$$E_s^{\text{sub}} = \frac{V N_{\perp}}{2} \sum_{q, \mu} \{2 - \cos[4\pi(\beta_q^{s, \mu} + \alpha_{\perp, q}^{s, \mu})]\}. \quad (93)$$

TABLE I: Numerical results for V_c^{PT} and optimal parameters $w_x = \alpha'_x/\alpha$, $w_y = \alpha'_y/\alpha$, and $s_y = \eta'/\eta$ for the PT-soliton evaluated at discrete angles θ determined by small Miller indices. The corresponding analytic results for the hexagonal and the bb' rhombic elasticity theories are $V_c^{\text{PT}} \approx 0.0416 e_D$ at $\theta \approx 42.13^\circ$ and $V_c^{\text{PT}} \approx 0.0417 e_D$ at $\theta \approx 45.05^\circ$.

| θ | V_c^{PT}/e_D | w_x | w_y | s_y |
|--------------|-----------------------|-------|-------|-------|
| 21.5° | 0.033 | 1.1 | 1.2 | 0.95 |
| 33.2° | 0.042 | 0.9 | 0.95 | 1.05 |
| 44.5° | 0.046 | 0.8 | 0.75 | 1.1 |
| 63.0° | 0.031 | 1.3 | 1.15 | 1.05 |
| 75.7° | 0.016 | 1.85 | 2.05 | 1 |

Repeating the calculation for the particle system without soliton ($\rightarrow E_{\triangleright'}^{\text{int}}, E_{\triangleright'}^{\text{sub}}$), the final expression for the soliton line energy per length a_1 is

$$\varepsilon = (E_s^{\text{int}} - E_{\triangleright'}^{\text{int}} + E_s^{\text{sub}} - E_{\triangleright'}^{\text{sub}} + p\delta A)/N_{\perp} a_1, \quad (94)$$

where the last term $p\delta A$ represents the cost due to the area change which comes along with the soliton deformation and depends on the direction of z ; for the PT-soliton with its lattice shift $\mathbf{d}^{\text{PT}} = (-b, s_y \eta b)$, we find the area change per l -strip (such that $\delta A = N_{\perp} \delta A_{m, n}^{\text{PT}}$)

$$\delta A_{m, n}^{\text{PT}} = a_1 (\mathbf{d}^{\text{PT}} \cdot \hat{\mathbf{e}}_z). \quad (95)$$

This area change is negative and hence the PT soliton involves a lattice compression, in agreement with the fact that the smaller density n' of the bb' lattice has to approach the larger density n of the hexagonal lattice when overlapping PT solitons approximate the distorted and rotated hexagonal phase at small V . For the PT soliton at $m = n = 2$ the area change is of order of 25 % of the supercell area, implying that about 1 particle is added to every two such cells along the soliton.

In order to verify the numerical accuracy, we have calculated the lattice energy $e_{\triangleright'}$ using the uniform version of Eq. (92) (without the soliton) and have compared it to the value $e_{\triangleright'} = 4.3489 e_D$ obtained with the help of the Ewald summation technique: Going up to $N = 25000$ particles (where $e_{\triangleright'} \approx 4.3465 e_D$) the value obtained from Ewald summation is approached with an error (due to boundary effects) vanishing as $1/N$. When calculating the properties of the soliton, we go up to system sizes with $N = 5000$ particles (corresponding to a system size $Z = N h_z/2$ along z with the height $h_z = bb'/2\sqrt{b^2 + b'^2}$ of the unit cell along z). This size is sufficiently large to produce results with an accuracy in the per mill range (note that boundary effects are less relevant in the energy differences (94) determining the soliton energy). Placing the soliton midway, $z_s = Z/2$, and varying the parameters w_x , w_y , and s_y , we find the first soliton entry where $\varepsilon = 0$ at the critical potential

$$V_c^{\text{PT}} \approx 0.046 e_D, \quad \theta \approx 44.5^\circ, \quad (96)$$

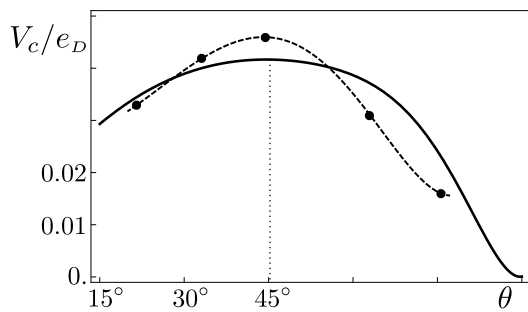


FIG. 13: Numerical results for the critical substrate potential V_c^{PT} of the PT-soliton at discrete angles defined by small Miller indices (black dots); the dashed line is a guide to the eye. The solid line is the analytic result based on the elastic description of the bb' rhombic lattice. The thin dotted line marks the optimal angle $\theta \approx 45.05^\circ$ where the analytic result assumes its maximal value $V_c^{\text{PT}} \approx 0.0417 e_D$.

appreciably larger than the result (84) of the analytic calculation. The optimal soliton parameters are $w_x \approx 0.8$, $w_y \approx 0.75$, and $s_y \approx 1.1$, i.e., the optimized soliton shape is narrower in both directions and the shift vector is larger along y , $\mathbf{d}^{\text{PT}} \approx (-b, 0.766b)$.

The calculation for the other Miller indices follows the same program as the one described above and the results are summarized in Table I; Fig. 13 shows the critical substrate potentials V_c^{PT} at the discrete angles for small Miller indices in comparison with the analytic results based on the elastic theory for the bb' rhombic lattice, with the critical potential at $\theta = 44.5^\circ$ being the largest.

VII. SOLITONS AND DOMAIN WALLS WITH TWO SUBSTRATE MODES

The soliton array obtained within the resonance approximation transforms the bb' rhombic lattice to the hexagonal one, while our goal here is to study the transformation of the particle system from square to hexagonal. The solitonic instability then should appear at small $V < V_\square$ on the background of the period-doubled phase, which requires us to include the second harmonic of the substrate potential into our analysis. We treat the period-doubled phase as a bb rhombic lattice distorted by the relative shift $\bar{\delta}$ of the two sublattices see Sec. III B. The soliton is described by a smooth displacement field $\mathbf{v}(\mathbf{R})$ relative to the bb lattice. Inside the soliton, the amplitude of the short-scale distortion $\bar{\delta} = (b/\pi) \arcsin[V \cos(qv_y)/8\Delta]$ is slaved to the displacement $\mathbf{v}(\mathbf{R}) = (b/4) \mathbf{e}_y + \bar{\sigma}$ which is replacing the scalar center of mass variable $\bar{\sigma}$ introduced above, see Eq. (29).

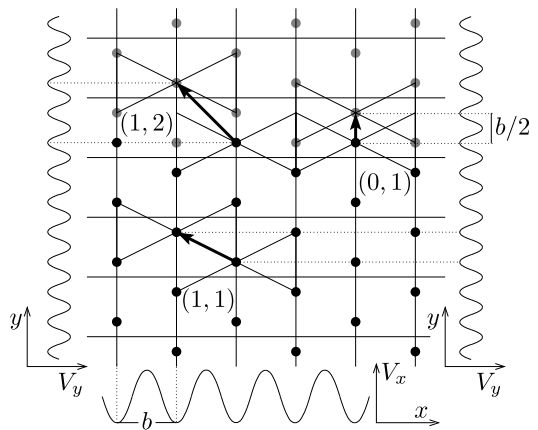


FIG. 14: Selection of low-energy solitons and domain-walls shifting the period-doubled lattice by $\mathbf{d}_{j,k} = (-jb, kb/2)$, $j, k \in \mathbb{Z}$, the topological vector-charge associated with the defect. The simplest defect is the $(0, 1)$ -domain wall crossing only the barrier along y and connecting different twins of the period-doubled phase. The $(1, 1)$ -soliton crosses both barriers along x and along y and connects identical twins. Finally, the domain-wall $(j, k) = (1, 2)$ crosses both potential barriers, once the barrier along x and twice that along y . Note that the barrier along y is reduced with respect to the barrier along x by the factor $V/32\Delta = V/4V_\square$.

We then have to minimize the energy³⁶

$$\delta g = \frac{1}{N} \int d^2 R \left\{ g_\square^{\text{el}}(\mathbf{v}) + \frac{Vn}{2} [1 - \cos(qv_x)] + \frac{nV^2}{64\Delta} [1 - \cos(2qv_y)] \right\}, \quad (97)$$

where g_\square^{el} is the elastic Gibbs free energy³⁷ density of the bb rhombic lattice describing the long wave-length distortions of the period-doubled lattice and δg denotes the deviation from $g_{\text{pd}}(V)$, Eq. (26).

While the resonance approximation admits only one low-energy soliton, the full problem with both substrate modes present allows for several types of line-defects with different quantized topological vector-charges $\mathbf{d}_{j,k} = (-jb, kb/2)$, $j, k \in \mathbb{Z}$. The latter correspond to the shift $\mathbf{d}_{j,k} = \mathbf{v}^{(j,k)}(\infty) - \mathbf{v}^{(j,k)}(-\infty)$ of the lattice associated with the defect, similar to the Burger's vector characterizing the displacement field of a dislocation. A selected set of defects with potentially low energies are shown in Fig. 14: promising candidates reminding about the PT soliton are the $(j, k) = (1, k)$ defects with $k = 1, 2, 3$, but a simple Ansatz with the shift $\mathbf{d}_{01} = (0, b/2)$ should be tried as well, since the particles merely have to overcome the weak effective potential $\propto V^2/64\Delta \ll V/2$ along the y -direction, see Eq. (97). All these line defects fall into two classes, the domain walls with odd values $j + k$ and taking the period-doubled phase from one twin to the other, $\delta \rightarrow -\delta$, and the genuine solitons with $j + k$ even and the same twin on both sides, $\delta \rightarrow \delta$, see Fig. 14.

When considering both substrate modes, the topological vector-charge $\mathbf{d}_{j,k} = (-j, k/2)b$ of the soliton array is quantized in both directions x and y . The global displacement field \mathbf{u}_g resulting from the soliton array then must be compatible with both quantization conditions along x and y . The (shear) displacement field taking the bb rhombic lattice³⁸ into the hexagonal one is given by $\mathbf{u}_g = (-\alpha_x x, \alpha_y y)$ with $\alpha_x = s/(1+s)$ and $\alpha_y = s$. Such a displacement field cannot be built from a single soliton array with the quantized geometrical constraint on $\mathbf{d}_{j,k}$ since $s = (4/3)^{1/4} - 1$ is an irrational number. Hence, the quantization of the topological-vector charge provides us with a valuable input on the square-to-hexagonal transition pathway: this pathway has to involve more than one soliton transition or another more complex route. As we will show below, the way the system will deal with this problem is by undergoing two transitions: in the first transition, involving a (0,1)-domain-wall, the mean lattice constant along y smoothly changes from b to b' as domain-walls flood the system, implying that the substrate potential along y is washed out (we remind that, for a 1D commensurate-incommensurate transition¹, the mean lattice constant $\langle a \rangle$ smoothly goes from b (in the locked phase) to a (in the free phase) as the substrate potential is reduced from the critical value V_c to zero). The resulting bb' rhombic lattice then undergoes a second soliton transition with the PT soliton array taking the rhombic lattice to the hexagonal phase by washing out the second substrate mode along x . Hence the two geometrical constraints on the locked phase are subsequently released by two consecutive transitions.

In the following, we search for line solitons directed along an angle θ using the Ansatz $\mathbf{v}(x, y) = \mathbf{v}(z)$ with $z = x \cos \theta + y \sin \theta$ and focus on their first appearance—the physically relevant topological defect then is that one with the largest critical substrate potential $V_c^{(j,k)}$. Again, we first analyze the problem within a continuum elastic theory and then refine our results with a numerical analysis.

A. Continuum elastic approach

Accounting for the boundary conditions, the energy (97) can be rewritten as the sum of a line energy ε_s and a drive ε_d . The line energy assumes the form (79) with the elastic coefficients $\gamma'_{x,y}$, $\kappa'_{x,y,xy}$, $\mu'_{x,y,xy} \rightarrow \gamma_{x,y}$, $\kappa_{x,y,xy}$, $\mu_{x,y,xy}$ replaced by those for the bb rhombic lattice, see appendix C for their evaluation. In addition, the double-periodic effective potential $(nV^2/64\Delta)[1 - \cos(2qv_y)]$ along y has to be accounted for, see (97). The drive replacing Eq. (80) reads

$$\varepsilon_d = -j(\gamma_x + p)b \cos \theta + \frac{k}{2}(\gamma_y + p)b \sin \theta \quad (98)$$

and includes an additional term along y .

The simplest case to evaluate is the (0,1) domain-wall with the displacement field directed along y , $\mathbf{v}(z) =$

$(0, v_y(z))$. The variation of the line energy produces a Sine-Gordon equation with the double-periodic potential along y and inserting the standard soliton solution $v_y = (b/\pi) \arctan[\exp(z/\sqrt{\alpha_\triangleright^y})]$ back into ε_s , we obtain the line energy

$$\varepsilon_s^{(0,1)} = \frac{nV^2}{8\Delta} \sqrt{\alpha_\triangleright^y} \quad (99)$$

with

$$\alpha_\triangleright^y = \frac{64\Delta}{nV^2} \frac{\kappa_y \sin^2 \theta + \mu_y \cos^2 \theta}{4q^2}. \quad (100)$$

Balancing this energy with the drive $\varepsilon_d = (\gamma_y + p)b \sin \theta/2$, we find the critical field

$$V_c^{(0,1)}(\theta) = -\frac{2\pi(\gamma_y + p)}{n} \sqrt{\frac{n\Delta}{\kappa_y + \mu_y \cot^2 \theta}}, \quad (101)$$

which is monotonically increasing with θ . The first (0,1) domain-wall then appears at

$$V_c^{(0,1)} \approx 0.0753 e_D, \quad \theta^{(0,1)} = 90^\circ. \quad (102)$$

Next, we analyze the $(1, k)$ solitons crossing the large barrier along x once and k times the small barrier along y . While in the resonance approximation the v_y displacement was slaved to the v_x field (see (82)), the potential $\propto V^2/\Delta$ along y renders the solution of the differential equations more difficult. Since the potential along y is small as compared to the one along x , $V^2/\Delta \ll V$, we seek a perturbative solution $\mathbf{v} = \mathbf{v}^{(0)} + \mathbf{v}^{(1)}$. To lowest order, we drop the potential along y and obtain the usual soliton solution

$$\begin{aligned} v_x^{(0)} &= -(2b/\pi) \arctan[\exp(z/\sqrt{\alpha_\triangleright^x})], \\ v_y^{(0)} &= -\eta_\triangleright v_x^{(0)}, \end{aligned} \quad (103)$$

with

$$\alpha_\triangleright^x = \frac{2}{nVq^2} \left[\kappa_x \cos^2 \theta + \mu_x \sin^2 \theta - \frac{(\kappa_{xy} + \mu_{xy})^2 \cos^2 \theta}{\kappa_y + \mu_y \cot^2 \theta} \right], \quad (104)$$

$$\eta_\triangleright = \frac{(\kappa_{xy} + \mu_{xy}) \cot \theta}{\kappa_y + \mu_y \cot^2 \theta}. \quad (105)$$

Including the potential along y , we have to solve the equation

$$\alpha_\triangleright^y \partial_z^2 (2qv_y) = \sin(2qv_y) - \alpha_\triangleright^y \eta_\triangleright \partial_z (\partial_z 2qv_x) \quad (106)$$

with α_\triangleright^y given in Eq. (100). Since typically $\alpha_\triangleright^x \ll \alpha_\triangleright^y$ the v_x -soliton is rather narrow and the expression $\partial_z v_x$ in (106) can be replaced by a δ -function, $\partial_z v_x \approx -b\delta(z)$; the displacement field v_y then can be found as the solution of the Sine-Gordon equation $\alpha_\triangleright^y \partial_z^2 (2qv_y) = \sin(2qv_y)$ with the additional boundary condition

$$v_y(0^+) - v_y(0^-) = \eta_\triangleright b. \quad (107)$$

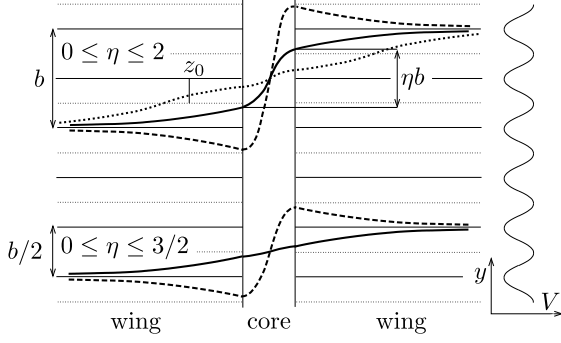


FIG. 15: Sketch of core ($v_y^{(0)}$) and wing ($v_y^{(1)}$) solutions for the $(1, k)$ -solitons for the cases $k = 2$ (top) and $k = 1$ (bottom). Solid lines are for $\eta_{\triangleright} < 1$ (top) and $\eta_{\triangleright} < 1/2$ (bottom); dashed lines are for $\eta_{\triangleright} \geq 1$ (top) and $\eta_{\triangleright} \geq 1/2$ (bottom); the dotted line (top) is for $\eta_{\triangleright} < 1/2$ where the solution approaches the shape of two consecutive solitons with shifts $b/2$ each. Within the core region, the v_x -soliton drags the v_y -soliton across the valley thereby binding the two wing solitons into a proper solution. Our analytic solution ignores the finite width of the core $v_y^{(0)}$.

The solution v_y thus splits into a combination of soliton solutions, the 0-order core part $v_y^{(0)} = -\eta_{\triangleright} v_x^{(0)}$ which we describe as a sharp jump (107) at the origin and a smooth ‘wing’ part $v_y^{(1)}$ of extended width $\sqrt{\alpha_{\triangleright}^y}$ taking the solution to the nearby potential minimum, see Fig. 15. The explicit form of the wings is given by the solutions

$$\begin{aligned} v_y^{(1)}(z > 0) &= \frac{kb}{2} \pm \frac{b}{\pi} \arctan[\exp[-(z + z_0)/\sqrt{\alpha_{\triangleright}^y}]], \\ v_y^{(1)}(z < 0) &= \mp \frac{b}{\pi} \arctan[\exp[(z - z_0)/\sqrt{\alpha_{\triangleright}^y}]], \end{aligned} \quad (108)$$

with

$$z_0 = -\sqrt{\alpha_{\triangleright}^y} \ln \left[\tan \left(\frac{\pi}{2} |\eta_{\triangleright} - k/2| \right) \right], \quad (109)$$

where the upper/lower signs apply to the cases $k/2 \leq \eta_{\triangleright} \leq (k+2)/2$ and $\max[(k-2)/2, 0] \leq \eta_{\triangleright} < k/2$, respectively; two representative cases for $k = 2$ and $k = 1$ are illustrated in Fig. 15. Note that the two wing solitons can cover at most a shift $\pm 2(b/2)$ along y ; these shifts, combined with the jump $\eta_{\triangleright} b$ in the core has to add up to the total shift $kb/2$ along y , what poses some restrictions on the allowed angles θ defining the direction of the z -axis.

It remains to determine the total line energy of the $(1, k)$ defect; inserting the solutions $v_x \approx v_x^{(0)}$ (we drop the shape correction $v_x^{(1)}$ induced by $v_y^{(1)}$) and $v_y \approx v_y^{(0)} + v_y^{(1)}$ into the expression for the line energy ε_s , we obtain the result

$$\varepsilon_s = 4nV \sqrt{\alpha_{\triangleright}^x} + \frac{nV^2}{64\Delta} 2 \int_0^{|u_0|} du \sqrt{2\alpha_{\triangleright}^y} \sqrt{1 - \cos u} \quad (110)$$

with $u_0 = 2qv_y^{(0)}(0^-) = \mp 4 \arctan[\exp(-z_0/\sqrt{\alpha_{\triangleright}^y})]$, see Eq. (108); the factor 2 before the integral accounts for the

TABLE II: Analytic (evaluated with the elastic theories for the bb rhombic and hexagonal (hex) lattices) and precise numerical (num) results for $V_c^{(j,k)}$ and optimal angles $\theta^{(j,k)}$.

| (j, k) | $V_c/e_D, bb$ | θ, bb | $V_c/e_D, hex$ | θ, hex | $V_c/e_D, num$ | θ |
|----------|---------------|--------------|----------------|---------------|----------------|----------|
| (0, 1) | 0.0753 | 90° | — | — | 0.0741 | 45° |
| (1, 1) | 0.0529 | 72.45° | 0.0309 | 58.7° | 0.0382 | 63.4° |
| (1, 2) | 0.0536 | 79.15° | 0.0478 | 47.8° | 0.0501 | 45° |
| (1, 3) | 0.0572 | 54.2° | 0.0447 | 45.3° | 0.0544 | 45° |

two wings at positive and negative z . The final results for the $k = 1, 2, 3$ solitons then are given by

$$\varepsilon_s^{(1,k)} = 4nV \sqrt{\alpha_{\triangleright}^x} + \frac{nV^2}{8\Delta} \sqrt{\alpha_{\triangleright}^y} (1 - \cos[\pi(\eta_{\triangleright} - k/2)]). \quad (111)$$

Obviously, the correction due to the wings vanishes when $\eta_{\triangleright} = k/2$, i.e., when the jump at the origin induced by $v_x^{(0)}$ already matches the imposed boundary condition set by the shift vector $\mathbf{d}_{j,k}$. The critical values for the substrate potentials V_c and optimal angles θ are then again found by (numerically) evaluating the points where the total line energies $\varepsilon(V, \theta) = \varepsilon_s(V, \theta) + \varepsilon_d(V, \theta)$ go to zero for the first time upon decreasing V and the results for the $(1, 1)$ and $(1, 3)$ solitons and for the $(1, 2)$ domain-wall are

$$V_c^{(1,1)} \approx 0.0529 e_D, \quad \theta^{(1,1)} \approx 72.45^\circ, \quad (112)$$

$$V_c^{(1,2)} \approx 0.0536 e_D, \quad \theta^{(1,2)} \approx 79.15^\circ, \quad (113)$$

$$V_c^{(1,3)} \approx 0.0572 e_D, \quad \theta^{(1,3)} \approx 54.2^\circ, \quad (114)$$

with a slight advantage for the $(1, 3)$ domain-wall but all values appreciably lower than the result (102) for the $(0, 1)$ domain-wall.

Since the soliton core of the $(1, k)$ defects are expected to have a structure close to the free hexagonal lattice, we have calculated the critical parameters using the elastic theory for the hexagonal lattice as well (the core of the $(0, 1)$ domain-wall resembles the bb' rhombic lattice, hence trying a hexagonal elastic theory is not promising). The results are summarized in Table II; the values for V_c calculated for the hexagonal lattice are systematically smaller and appreciably different from those obtained via the bb elastic theory. Once more, we conclude that a numerical analysis is required in order to faithfully compare the energies of the various topological defects and determine the type and critical potential for the best candidate.

B. Numerical analysis

Our numerical analysis for the $(0, 1)$ and $(1, k)$ defects makes use of the quantization of the topological vector

charge $\mathbf{d}_{j,k}$: the return of the particles to original lattice points after the passage of one soliton (or two domain walls) allows us to analyze a periodic array of defects, thereby reducing the problem of boundary effects and large system size. As a result, rather than a variational, we will be able to perform a full relaxation of the soliton shape and thus attain more precise results. In the following, we first analyze the simplest situation, the (0,1) domain-wall at $\theta = 90^\circ$ and then extend the discussion to other (discrete) angles. Subsequently, we study the (1, k) defects for $k = 1, 2, 3$; the results are summarized in Table II together with the analytic results. New elements in the analysis will be introduced on the go and not repeated for every case.

1. (0,1) domain-wall at $\theta = 90^\circ$

In order to understand the impact of a finite system size and the interaction between defects, we first analyze a crude model describing two (0,1) domain-walls in terms of two missing rows of particles separated by $2y_s$ in a system of size $2Y$. We start from the bb rhombic lattice and consider two rows separated by the distance y . Summing the interaction over the x -coordinates (with N_\perp the number of unit cells of size $2b$ along x) and using Eq. (91), we find the interaction energy between the two rows at the distance y

$$E_{>}^{\text{int}}(y) = N_\perp e_D \sum_l \frac{b^3}{[(2bl)^2 + y^2]^{3/2}} \approx N_\perp e_D \frac{b^2}{y^2},$$

where we have ignored corrections due to the sum over \bar{l} in (91) (this approximation, i.e., replacing the sum over l by an integral, is valid at large $y/b \gg 1$). With the shift vector $\mathbf{d}_{0,1} = (0, b/2)$, we can describe the two domain walls by shifting all rows with $y > y_s$ ($y < -y_s$) up (down) by a distance $b/2$. Summing the interaction energies over all rows including these shifts and substrating the sum without shifts we obtain the interaction part of the two defect lines in the form (we divide by $N_\perp 2b$ to obtain a line energy)

$$\varepsilon \approx \frac{e_D}{a_1} \frac{4}{2} \left[\sum_{j \neq j'}^{2s} - \sum_{j \neq j'} \right] \frac{1}{(j - j')^2}, \quad (115)$$

with $y = jb/2$, $b/2$ the distance between rows along the y direction and the factor $1/2$ avoids double counting of rows. In Eq. (115) the sum \sum^{2s} has to be taken between $\pm j_Y = \pm(2Y/b + 1)$ but with $j, j' \neq \pm j_s = \pm 2y_s/b$ (we consider a symmetrized situation which provides equal leading corrections from the two solitons), while the second sum goes over $j, j' = -(j_Y - 1), \dots, (j_Y - 1) = -2Y/b, \dots, 2Y/b$. Then the following terms survive the

cancellation in the difference of sums,

$$\varepsilon \approx \frac{4e_D}{a_1} \left\{ \sum_{j \neq \pm j_s} \left[\frac{1}{(j_Y - j)^2} + \frac{1}{(j_Y + j)^2} \right] - \sum_j \left[\frac{1}{(j_s - j)^2} + \frac{1}{(j_s + j)^2} \right] - \frac{1}{(2j_Y)^2} + \frac{1}{(2j_s)^2} \right\}, \quad (116)$$

where the additional factor 2 arises from interchanging the role of j and j' and the last two terms correct for double counting the interactions between the ‘adatoms’ at $\pm j_Y b$ and ‘vacancies’ at $\pm j_s b$; self-energy terms always have to be dropped from the sums. Replacing the sums by integrals, e.g.,

$$\sum_j \frac{1}{(j_s \pm j)^2} \approx \left[\int_{-j_Y+1}^{\mp j_s-1} + \int_{\mp j_s+1}^{j_Y-1} \right] \frac{dx}{(j_s \pm x)^2} \quad (117)$$

$$= 2 - \frac{1}{j_Y - 1 - j_s} - \frac{1}{j_Y - 1 + j_s},$$

we can evaluate Eq. (116) and obtain the asymptotic behavior (we assume $j_s \ll j_Y$ and drop terms $\propto j_Y^{-2}$)

$$\varepsilon \approx \varepsilon^\infty + \frac{e_D}{a_1} \left(\frac{4b}{Y + y_s} + \frac{4b}{Y - y_s} - \frac{2b}{Y} + \frac{b^2}{4y_s^2} \right). \quad (118)$$

The result (118) shows that boundary effects decay with inverse system size $\propto 1/2Y$, while the interaction between defects decays faster, as the inverse square of the defect separation $2y_s$. It is the long-range interaction $\propto 1/R^3$ between particles that enhances the defect interaction, from the usual exponential behavior (see (68)) to an inverse-square law³⁵; the non-dispersive elastic theories did not catch this effect in our previous analytic studies. Regarding our numerical studies, we learn that analyzing periodic systems allows us to avoid boundary effects which decay only slowly $\propto 1/Y$; furthermore, working with a system size $Y \sim 100b$, the residual interaction between solitons contributes a small error of order $10^{-4} e_D/a_1$ to the isolated defect energy. These small system sizes then allow us to fully relax the defect shapes.³⁹

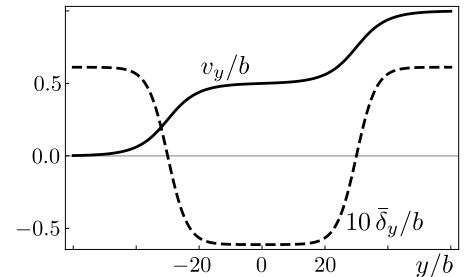


FIG. 16: Shape of two (0,1)-solitons $v_y(y)/b$ as well as internal distortion $\delta_y(y)/b$ for $V = 0.075_D$. The soliton width is $\sqrt{\alpha_y} \approx 6.1b$. The distortion field $\delta_y(y)$ (dashed) is expanded by a factor 10 for better visibility.

The implementation with periodic boundary conditions profits from an alternative particle enumeration with only one index (at fixed strip index l). The particle positions of the bb rhombic lattice are chosen as

$$\mathbf{R}_{lj}^{\triangleright} = \begin{pmatrix} la_1 + x_j \\ y_j \end{pmatrix}, \quad (119)$$

with $x_j/b = (1 + (-1)^j)/2$ referring to the alternating columns in the doubled unit cell and $y_j/b = j/2 - 1/4$. The coordinates of the period-doubled lattice are $\mathbf{R}_{lj}^{\text{pd}} = \mathbf{R}_{lj}^{\triangleright} + (0, (-1)^j \bar{\delta}_y/2)$ with $\bar{\delta}_y = (b/\pi) \arcsin(V/8\Delta)$, see Eq. (31), and including two domain-walls at y_{s_1} and y_{s_2} with the displacement and distortion fields $v_y(y)$ and $\bar{\delta}_y(y)$ (see Fig. 16)

$$v_y(y) = (b/\pi) \left\{ \arctan[\exp[(y - y_{s_1})/\sqrt{\alpha_y}]] + \arctan[\exp[(y - y_{s_2})/\sqrt{\alpha_y}]] \right\}, \quad (120)$$

$$\bar{\delta}_y(y) = (b/\pi) \arcsin[(V/8\Delta) \cos[2\pi v_y(y)/b]], \quad (121)$$

we obtain the coordinates of the particles in the defected lattice $\mathbf{R}_{lj}^s = \mathbf{R}_{lj}^{\triangleright} + (0, v_y(y_j) + (-1)^j \bar{\delta}_y(y_j)/2)$. Working with periodic boundary conditions, the cell size L has to be chosen such that the boundaries match. For the $(0, 1)$ domain-wall and $\theta = 90^\circ$ this is easily satisfied for $L/b \in \mathbb{N}$ and two domain-walls per period placed at the positions $y_{s_1} = L/4 - b/4$ and $y_{s_2} = 3L/4 - b/4$, taking the lattice from the twin A phase to the twin B phase and again back to twin A, see Fig. 17.

The calculation of the interaction energy (92) is modified by splitting the sum over particle distances $y_{jj'} = y_j - y_{j'}$ in a sum over particle distances within one period and then extend the sum over periodic images. This corresponds to changing the $2/\beta^2$ term in the interaction (91) to $\sum_k 2/(\beta + kL/a_1)^2 = [2(\pi a_1/L)/\sin(\pi \beta a_1/L)]^2$ and replace the argument in the correction terms by $\beta^{\text{min}} = \min[\beta, L/a_1 - \beta]$ (due to the exponential decay of $K_1(y)$ at most the image in the neighboring cell might contribute). The interaction energy (92) finally assumes the form (with $\ell = L/a_1$ and $\alpha_{jj'}^s, \beta_{jj'}^s$ the relevant scaled difference coordinates, cf. Sec. VIB)

$$E_s^{\text{int}} = \frac{N_{\perp} D}{a_1^3} \sum_{j'=1}^N \left\{ \frac{4}{\ell^2} \zeta(2) + \sum_{j=1 < j'} \left[\frac{2(\pi/\ell)^2}{\sin^2(\pi \beta_{jj'}^s/\ell)} + 8\pi \sum_{\bar{l} > 0} \bar{l} \cos(2\pi \bar{l} \alpha_{jj'}^s) \frac{K_1(|2\pi \bar{l} \beta_{jj'}^{s, \text{min}}|)}{|\beta_{jj'}^{s, \text{min}}|} \right] \right\}, \quad (122)$$

where the first term accounts for the interaction between a particle and its periodic images. The accommodation of the substrate energy E_s^{sub} , see Eq. (93), to the new situation is straightforward and the area change associated with the two domain-walls with shifts $b/2$ is $\delta A = 2a_1 b/2 = 2b^2$.

Our numerical study involves a system size $L = 401b$ and 15 relaxational steps, resulting in a precision of $a_1 \delta \varepsilon / e_D \sim 10^{-4}$ (note that the precise shift $\bar{\delta}_y$ has to

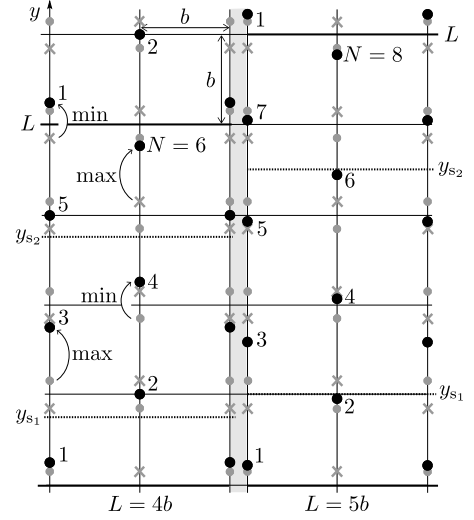


FIG. 17: Displaced particles (black dots) for a period-doubled lattice with two domain walls at $y_{s_1} = L/4 - b/4$ and $y_{s_2} = 3L/4 - b/4$. The domain walls take the period-doubled lattice from the twin A (grey points) to the twin B phase (grey crosses) and back to the original lattice. Periodicity is trivially achieved with $L/b \in \mathbb{N}$; examples are shown for $L = 4b$ with 6 particles (left) and $L = 5b$ (right). Particles with odd index j first cross a substrate maximum (max) shifting by $b/2 + \bar{\delta}_y$ and then a minimum (min, shifting by $b/2 - \bar{\delta}_y$) while particles with even j 's have the reversed order.

be found by numerical relaxation as well). The initial analytic solution with width $\sqrt{\alpha_y^y} \approx 6.1b$ relaxes only minimally (not visible in Fig. 18(a); the relaxation itself shown in Fig. 18(b) is of the order of $10^{-2}b$ and is larger when particles cross a minimum). The unrelaxed critical potential $V_c^{(0,1), \text{ur}} \approx 0.0730 e_D$ increases by a small amount to the relaxed value

$$V_c^{(0,1)} \approx 0.0732 e_D, \quad \theta = 90^\circ. \quad (123)$$

2. $(0, 1)$ domain-wall at other angles

The analytic result Eq. (101) for the critical substrate potential of the $(0, 1)$ domain-wall depends weakly on angle, with a flat maximum at $\theta = 90^\circ$. Here, we find the angle dependence of $V_c^{(0,1)}$ for discrete angles $\theta = \arctan(m/n)$ belonging to small Miller indices (m, n) , using the methodology in Sec. VIB adapted to the bb rhombic lattice and making use of the numerical relaxation of the defect shape as in Sec. VIIB1. The four cases analyzed below are illustrated in Fig. 19. The change in area δA (or ‘charge’ $Q = -\delta A/b^2$) associated with a domain-wall depends on the angle θ ,

$$\delta A_{m,n}^{(0,1)} = a_1 (\mathbf{d}_{0,1} \cdot \hat{\mathbf{e}}_z(\theta)) = (m/2)b^2, \quad (124)$$

and describes defects diluting the particle lattice (as opposed to the compressive PT soliton in Sec. VIB).

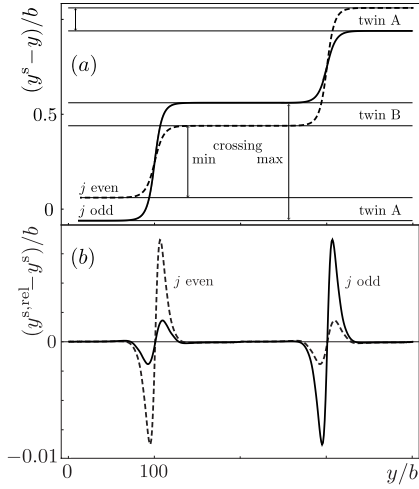


FIG. 18: (a) The displacement $y^s - y$ associated with two $(0, 1)$ domain-walls evaluated at $V = V_c^{(0,1)} = 0.0732 e_D$ after relaxation. When going from twin A to twin B, particles with odd index j (solid lines, shift by $b/2 + \bar{\delta}_y$) have to overcome a substrate maximum while the even j 's (dashed lines, shift by $b/2 - \bar{\delta}_y$) cross a substrate minimum (and vice versa from twin B back to twin A, see also Fig. 17). (b) Relaxation of the two domain-walls during 15 iterations. The maximal shift is on the level of $0.01 b$, symmetric around the defect center and more than 4.5 times larger when particles cross a substrate minimum than when crossing a substrate maximum.

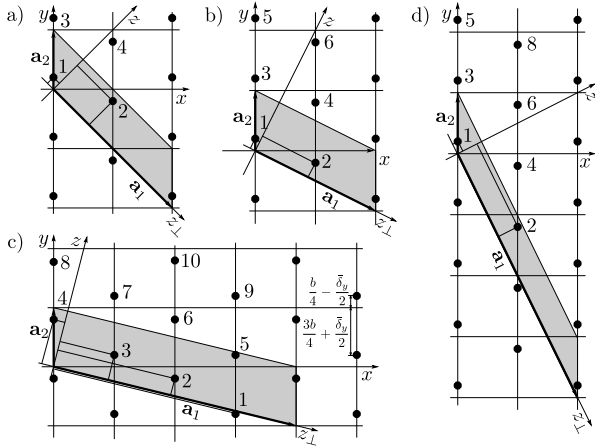


FIG. 19: Coordinates z_{\perp} and z for a) $\theta = 45^\circ$ ($(m, n) = (2, 2)$), b) $\theta \approx 63.4^\circ$ ($(m, n) = (2, 1)$), c) $\theta \approx 76.0^\circ$ ($(m, n) = (4, 1)$), and d) $\theta \approx 26.6^\circ$ ($(m, n) = (2, 4)$) describing the period-doubled lattice (shown as black dots) and an array of domain-walls evolving along z . For such uniaxial displacement fields along the z -axis, the structure remains invariant under a translation by the vector \mathbf{a}_1 ; choosing the unit cells (grey areas) with $2(4)$ particles allows for the summation of the interactions along z_{\perp} with period a_1 .

An important but not straightforward element is the choice of the periodic supercell. Correct matching after

the period L (or number of particles N) requires that

$$z_{\perp, N+1} = z_{\perp, 1} + p a_1, \quad z_{N+1} = z_1 + L \quad (125)$$

for some integer p . Note that this condition does not require that equal twins match up after one period, hence the number of defects per period can be one or two. Figure 20 illustrates two cases for $\theta = 45^\circ$ with $N_s = 3$ and $N_s = 11$ particles per unit cell, where $N_s = N_{pd} + n_s Q$ is the particle number per supercell in the presence of n_s defects with ‘charge’ Q and N_{pd} is the particle number in the undistorted supercell. For the angle $\theta = 45^\circ$ the allowed supercell lengths are given by $L/b = \sqrt{2}(2k + 1)$ with $k \in \mathbb{N}$; the allowed values for the other angles are given in Table III.

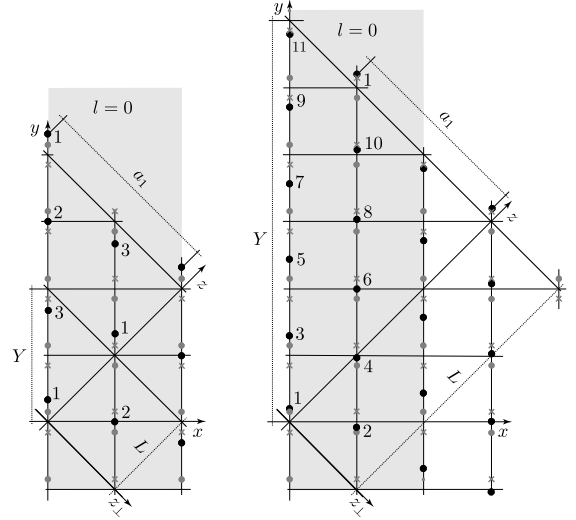


FIG. 20: Particle positions for the $(0, 1)$ -soliton at $\theta = 45^\circ$. One soliton ($n_s = 1$) per period $L = \sqrt{2}(2k + 1)b$ with $k \in \mathbb{N}$ already ensures correct matching at the boundaries as illustrated here for the cases $k = 0$ (left, shown are two periods of length $L = \sqrt{2}b$ containing $N_s = 3$ particles) and $k = 1$ (right, shown is one period of length $L = 3\sqrt{2}b$ with $N_s = 11$ particles). The shaded area corresponds to the $l = 0$ -strip. The particle number N_s per period is related to L via the ‘vertical period’ Y (and the charge Q per soliton), $L = Y \sin \theta$ and $N_s = 2Y/b + n_s Q$. Grey dots and crosses denote twin A and twin B lattice sites, respectively.

The angle $\theta \approx 63.4^\circ$ associated with the Miller indices $(2, 1)$ involves an additional subtlety: indeed, for this angle the summation over l in Eq. (91) can lead to (nearly) coinciding particle rows where β becomes small or even vanishes. This is the case when the internal distortion field $\bar{\delta}_y$ crosses zero within a domain-wall and the separation $z_{2q}^s - z_{2q-1}^s$ between the particles $j = 2q - 1$ and $j' = 2q$ vanishes. This spurious divergence can be dealt with in different ways, e.g., with the help of the Euler-

TABLE III: Parameters [cell sizes L ($k \in \mathbb{N}$), number of defects n_s per cell, and charge Q per defect (and length a_1)] for the numerical analysis of the (0,1) domain-wall for discrete angles θ and numerical results for the critical substrate strengths $V_c^{(0,1)}$ for the (0,1) domain-wall before (superscript ‘ur = unrelaxed’) and after relaxation. L and n_s are not independent quantities and may be chosen differently.

| θ | L/b | n_s | Q | $V_c^{(0,1),ur}/e_D$ | $V_c^{(0,1)}/e_D$ |
|----------|-------------------|-------|-----|----------------------|-------------------|
| 26.6° | $\sqrt{5}(2k+1)$ | 2 | -1 | 0.0684 | 0.0730 |
| 45° | $\sqrt{2}(2k+1)$ | 1 | -1 | 0.0718 | 0.0741 |
| 63.4° | $2\sqrt{5}(2k+1)$ | 2 | -1 | 0.0727 | 0.0735 |
| 76.0° | $\sqrt{17}(2k+1)$ | 1 | -2 | 0.0729 | 0.0733 |
| 90° | $2k+1$ | 2 | -1 | 0.0730 | 0.0732 |

Maclaurin formula

$$\begin{aligned} \sum_{l=-\infty}^{\infty} \frac{1}{[(l+a)^2 + \beta^2]^{3/2}} &\approx \sum_{l=-N+1}^{N-1} \frac{1}{[(l+a)^2 + \beta^2]^{3/2}} \\ &+ \frac{1}{\beta^2} \left(1 - \frac{N+a}{[(N+a)^2 + \beta^2]^{1/2}}\right) + \frac{1}{\beta^2} \left(1 - \frac{N-a}{[(N-a)^2 + \beta^2]^{1/2}}\right) \\ &+ \frac{1}{2} \frac{1}{[(N+a)^2 + \beta^2]^{3/2}} + \frac{1}{2} \frac{1}{[(N-a)^2 + \beta^2]^{3/2}} \\ &+ \frac{1}{4} \frac{N+a}{[(N+a)^2 + \beta^2]^{5/2}} + \frac{1}{4} \frac{N-a}{[(N-a)^2 + \beta^2]^{5/2}} + \dots \end{aligned}$$

where in the limit $\beta \rightarrow 0$ the first two correction terms should be replaced by $1/[2(N \pm a)^2]$.

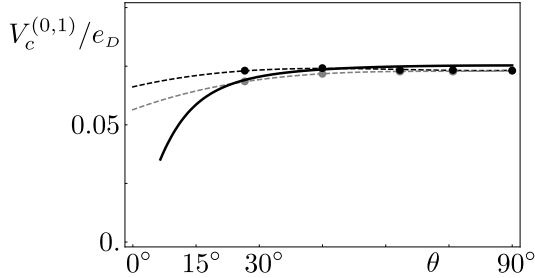


FIG. 21: The critical substrate strength $V_c^{(0,1)}$ for the (0,1) domain-wall as a function of θ . Upon relaxation the maximum shifts from $\theta = 90^\circ$ (grey points are numerical results using the analytic soliton shape) to $\theta = 45^\circ$; the angle dependence of the relaxed configuration (black dots) is very flat. The dashed lines are guides to the eye. The solid line shows the analytic result from the continuum elastic description, see Eq. (101).

Accounting for all these measures, the optimal domain-wall shapes are found numerically and the critical substrate potentials can be determined. The results are summarized in Table III and are illustrated in Fig. 21. Quite surprisingly, the optimal domain-wall does not appear at the symmetric angle $\theta = 90^\circ$ but rather far away near

$\theta \approx 45^\circ$, an angle that is unrelated to the symmetry axes of the parent crystal.

3. (1, k) defects

Next, we analyze defects with a displacement field that includes a component along the x -direction. We start out with the (1,2) domain-wall shifting the particles by a vector $(-b, b)$. The analytic expressions for the displacements describing the body (103) and wings (108) of the defect are illustrated in Fig. 22; furthermore, the intracell distortion $\bar{\delta}_y(z)$ as given by Eq. (121) is quite different from the one of the (0,1) domain wall as v_y increases by b across one domain wall (instead of $b/2$ in the (0,1) defect). As a result, the deformation is maximal and of opposite sign in the core and returns to its original value behind the defect, see Fig. 22, while for the (0,1) domain-wall this deformation vanished in the defect center and finally changed sign across the defect, thereby taking the particles to a different twin, see Fig. 16. On the contrary, it is the shift along x which leads to the different twin after crossing the (1,2) defect.

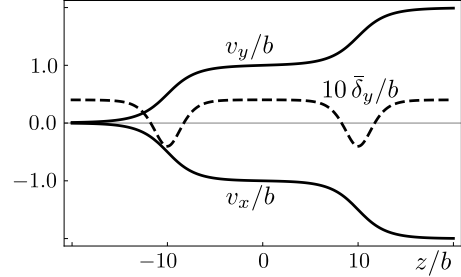


FIG. 22: Displacements $v_x(z)/b$ and $v_y(z)/b$ associated with the (1,2)-soliton and the corresponding internal distortion field $\bar{\delta}_y(z)/b$ for $V = 0.05 e_D$. The soliton widths are $\sqrt{\alpha_x} \approx 1.9b$ and $\sqrt{\alpha_y} \approx 6.6b$; within the soliton core, v_y rapidly changes by $\eta b \approx 0.94b$, leaving only small wing amplitudes. The distortion field $\bar{\delta}_y$ (dashed) is expanded by a factor 10 for better visibility.

Another peculiarity of the (1,2) domain-wall is its areal change $\delta A_{m,n}^{(1,2)} = a_1 (\mathbf{d}_{1,2} \cdot \hat{\mathbf{e}}_z(\theta)) = (m-n)b^2$ or ‘charge’ $Q = n - m$ which changes sign at $\theta = 45^\circ$ —the 45° domain-wall then is uncharged, while the one at $\theta \approx 26.6^\circ$ with $(m, n) = (2, 4)$ is a compression defect with $Q = 2$.

We make again use of a periodic arrangement of defects with the period L of the supercell chosen appropriately, see Fig. 23 for a sketch of two (1,2) domain-walls at $\theta = 45^\circ$ with $L = 2\sqrt{2}b$ and $N_s = 8$ particles and Table IV for a summary of suitable sizes L . Next, we determine the critical substrate potentials at the various discrete angles θ . We optimize the domain-wall shapes by numerical relaxation of the initial analytical solution and obtain the results listed in Table IV; figure 24 compares the results from the analytic solution with those obtained

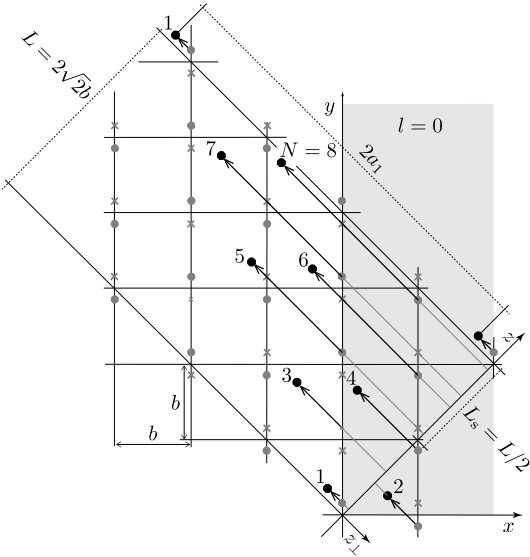


FIG. 23: Sketch of two (1,2)-solitons (of width L_s) within the period $L/b = 2\sqrt{2}$ ($N = 8$, i.e., four particles per soliton) going from twin A (grey dots) to twin B (grey crosses) and back to twin A. The shaded area corresponds to the $l = 0$ strip. With $(z_{\perp, N+1} - z_{\perp, 1}) = -2a_1$ the boundary condition (125) is properly satisfied. Grey dots and crosses denote twin A and twin B lattice sites, respectively.

numerically without and with relaxation. We find that the best (1,2) defect is directed close to $\theta = 45^\circ$ with $V_c^{(1,2)} \approx 0.0501 e_D$.

An interesting feature of the (1,2) domain wall reveals itself for the angles $\theta \approx 76^\circ$ and $\theta = 90^\circ$. Indeed, for the 76° angle, the relaxation process, although still converging, lasts much longer. While the initial displacement v_x along x remains nearly unchanged, the displacement v_y along y changes quite appreciably. In fact, the relaxation tends to dissolve the (1,2) defect into a (1,0) and a (0,2) part where the latter one tends to split into a domain-wall pair $(0,1) + (0,1)$, resembling the sketch in figure 15 (dotted line). However, at 76° the three parts still remain bounded and the relaxation converges. This is no longer the case at 90° where the relaxation never converged (explaining for the missing entry of a value for $V_c^{(1,2)}$ in table IV). We note that the (1,0) defect is compressing the lattice and hence involves a positive ‘charge’, while the (0,1) defects are diluting the lattice and hence are negatively charged. These oppositely charge defects then tend to bind into a cluster. However, the (1,0) defect becomes pure shear when θ approaches 90° , supporting the interpretation for a complete dissolution of the (1,2) soliton into a regular array of $(0,1) + (1,0) + (0,1)$ defects at 90° .

Finally, we briefly report on our study of the (1,1) and (1,3) solitons. The (1,3) soliton extends over a large distance $3b/2$ along the y -direction, of which a distance $b/2$ has to be covered by the core, requiring that $\eta > 1/2$ and

TABLE IV: Parameters [cell sizes L ($k \in \mathbb{N}$), number of defects n_s per cell, and charge Q per defect (and length a_1)] for the numerical analysis of the (1,2) domain-wall for discrete angles θ and numerical results for the critical substrate strengths $V_c^{(1,2)}$ for the (1,2) domain-walls before (superscript ‘ur = unrelaxed’) and after relaxation. L and n_s are not independent quantities and may be chosen differently.

| θ | L/b | n_s | Q | $V_c^{(1,2),ur}/e_D$ | $V_c^{(1,2)}/e_D$ |
|--------------|-------------------|-------|-----|----------------------|-------------------|
| 26.6° | $\sqrt{5}(2k+1)$ | 2 | 2 | 0.0253 | 0.0255 |
| 45° | $2\sqrt{2}(2k+1)$ | 2 | 0 | 0.0468 | 0.0501 |
| 63.4° | $\sqrt{5}(2k+1)$ | 1 | -1 | 0.0456 | 0.0492 |
| 76.0° | $\sqrt{17}(2k+1)$ | 1 | -3 | 0.0413 | 0.0441 |
| 90° | $2k+1$ | 2 | -2 | 0.0332 | – |

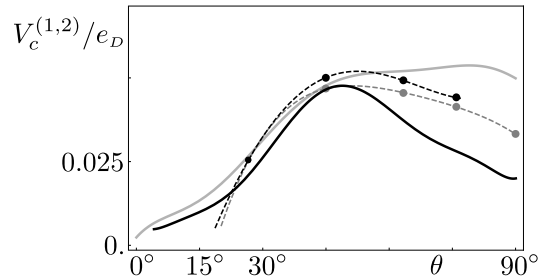


FIG. 24: The critical substrate strength $V_c^{(1,2)}$ of the (1,2) domain-wall as a function of θ . Grey points show the numerical results using the (unrelaxed) defect shape obtained analytically, black points are the values after relaxation. The dashed lines are guides to the eye. The black solid line is the analytic result obtained with the elastic theory for the hexagonal lattice, the grey solid line is the analytic result using the rhombic elasticity theory, see Sec. VII.

thereby restricting the allowed angles θ , see the discussion in Sec. VII. Another special case is the (1,1) soliton at $\theta \approx 26.6^\circ$, where $\eta \approx 1.4$ is large and nearly fully developed wing-solitons are needed to bring the v_y -overshoot in the core back to the imposed shift $b/2$. Such extensive wings require very large periods (soliton separations) in order to minimize the soliton-soliton interaction. Relaxing the soliton shape then necessitates a lot of computing time and we have abstained from its detailed study as this direction is not favorable anyway.

The supercell lengths L for the periodic arrays used in the numerical relaxation are summarized in Table V and the final results for the critical substrate potentials are presented in Table VI. Similar to the (1,2) domain-wall, the (1,3) soliton dissociates into elementary solitons $(1,3) \rightarrow (0,1) + (1,1) + (0,1)$ for large angles (the (1,3) defect is pure shear type at $\theta \approx 63.4^\circ$ and thus has zero ‘charge’).

Quite surprisingly, it is still the rather large (1,3) soliton that turns out as the best (1, k) defect with the highest critical substrate potential $V_c^{(1,3)} \approx 0.0544 e_D$ at

TABLE V: Parameters [cell sizes L ($k \in \mathbb{N}$), number of defects n_s per cell, and charge Q per defect (and length a_1)] for the numerical analysis of the (1, 1) and (1, 3) solitons at discrete angles θ .

| θ | (1,1) | | | (1,3) | | |
|--------------|--------------------|-------|-----|--------------------|-------|-----|
| | L/b | n_s | Q | L/b | n_s | Q |
| 26.6° | $\sqrt{5}k$ | 1 | 3 | $\sqrt{5}k$ | 1 | 1 |
| 45° | $2\sqrt{2}k$ | 1 | 1 | $2\sqrt{2}k$ | 1 | -1 |
| 63.4° | $4\sqrt{5}k$ | 2 | 0 | $2\sqrt{5}k$ | 1 | -2 |
| 76.0° | $2\sqrt{17}(2k+1)$ | 1 | -1 | $2\sqrt{17}(2k+1)$ | 1 | -5 |
| 90° | k | 1 | -1 | k | 1 | -3 |

TABLE VI: Numerical results for the critical substrate amplitudes before ('ur = unrelaxed') and after relaxation of the soliton shape for the (1, 1) and the (1, 3) solitons.

| θ | $V_c^{(1,1),ur}/e_D$ | $V_c^{(1,1)}/e_D$ | $V_c^{(1,3),ur}/e_D$ | $V_c^{(1,3)}/e_D$ |
|--------------|----------------------|-------------------|----------------------|-------------------|
| 26.6° | 0.0140 | | 0.0328 | 0.0337 |
| 45° | 0.0267 | 0.0287 | 0.0493 | 0.0544 |
| 63.4° | 0.0357 | 0.0382 | 0.0544 | – |
| 76.0° | 0.0332 | 0.0350 | – | – |
| 90° | 0.0249 | 0.0266 | – | – |

$\theta = 45^\circ$. However, this value is appreciably below the critical potential $V_c^{(0,1)} \approx 0.0741 e_D$ for the (0, 1) domain-wall at $\theta = 45^\circ$.

VIII. TRANSFORMATION PATHWAY FROM SQUARE TO TRIANGULAR

The following scenario then describes the transition from the square lattice to the hexagonal phase with decreasing substrate potential, see Fig. 1: Starting out at large substrate potential, the square lattice first undergoes a smooth transition at $V_\square \approx 0.2 e_D$ to a period-doubled zig-zag phase, thereby spontaneously breaking the x - y symmetry and selecting a strongly modulated direction (in this paper always chosen along x), leaving a weakly modulated double-periodic effective potential along the other direction (here, along y). This period-doubled lattice appears in two twin versions, where one twin transforms into the other by a shift b along x .

At $V_c^{(0,1)} \approx 0.0741 e_D$ the (0, 1) domain walls directed along $\theta \approx 45^\circ$ enter the period-doubled lattice. As these dilution defects start overlapping, they wash out the flat double-periodic substrate potential along y , giving way to the bb' rhombic phase. The bb' rhombic lattice then provides the proper parent lattice for the appearance of the Pokrovsky-Talapov solitons at $V_c^{\text{PT}} \approx 0.046 e_D$ near the angle $\theta \approx 44.5^\circ$. At this value of the substrate potential, the (0, 1) domain-wall phase has approached the

bb' -lattice to within $\approx 10\%$, as measured by the ratio of amplitudes \tilde{A} of the periodic displacement $\tilde{\mathbf{v}}$ generated by the (0, 1) domain wall array at different substrate potentials, $\tilde{A}(V_c^{\text{PT}})/\tilde{A}(V_c^{(0,1)}) = 0.019/0.25 \approx 0.08$ (the average misfit $(\langle b' \rangle - b)/b$ differs by $\approx 3\%$ from the asymptotic value $(b' - b)/b$, $(\langle b' \rangle - b')/(b' - b) \approx 0.03$, see Fig. 25). The proliferation of PT solitons then smoothly eliminates the x -harmonic and completes the transition to the distorted and rotated hexagonal lattice at small V .

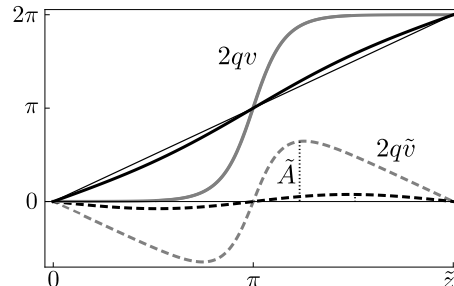


FIG. 25: Displacements v and \tilde{v} for the (0, 1) defect array as a function of \tilde{z} at different substrate potential strengths. Shown here are the total (dimensionless) displacement field $2qv = \tilde{z} + 2q\tilde{v}$ (solid lines) and its periodic part $2q\tilde{v}$ (dashed lines, with amplitudes \tilde{A}) for the (0, 1) soliton phase at $V \approx 0.046 e_D$ (black curves) and $V \approx 0.075 e_D$ (grey curves). The shapes are obtained from the analytic calculation using the bb' rhombic elasticity. The large decrease of \tilde{A} with decreasing V shows that at $V_c^{\text{PT}} \approx 0.046 e_D$ the bb' rhombic lattice is already established to within 10%.

IX. SUMMARY AND CONCLUSION

We have studied the competition between different lattice structures in a two-dimensional particle system with long-range dipolar interaction. Assuming an underlying substrate potential with square symmetry, the latter is in competition with the hexagonal lattice favored by the isotropic repulsion between particles. This setup generalizes the famous Frenkel-Kontorova model¹⁵ in one dimension where the competition is between two incommensurate lattice constants a for the particle system and b for the periodic substrate potential. In two dimensions, besides different lattice constants for the particle- and substrate lattice, the two systems also may involve different lattice symmetries—this is the case in the present study.

An important degree of freedom is the applied pressure p (or chemical potential μ) determining the particle density; here, we have chosen a situation with a commensurate density, i.e., the same density n of free particles and density of minima in the substrate potential $n = 1/b^2$, defining an appreciable misfit $s = b/h - 1 = 0.0746$ between the two lattices. We have studied the purely classical system free of any fluctuations, either quantum or

thermal, thus providing the starting point for later studies of the full dynamical phase diagram including fluctuations and external drive. The regime of validity of our results has to be checked case by case by comparing the interaction energy e_D with the quantum recoil ($e_r = \hbar^2 \pi^2 / 2mb^2$) and thermal energies ($k_B T$). Critical values for the quantum¹³ and classical⁴⁰ phase transitions between lattice and fluid are $r_Q = e_D / e_r \approx 18$ and $r_T = e_D / k_B T \approx 11$.

We have found the complete pathway taking the locked square lattice at large substrate potential V to the floating hexagonal phase at zero V . This includes a first transition at $V_\square \approx 0.2 e_D$ to a period-doubled zig-zag phase, a transition to a non-uniform phase with $(0,1)$ domain walls at $V_c^{(0,1)} \approx 0.0741 e_D$ approaching the bb' rhombic phase, and a second solitonic transition at $V_c^{\text{PT}} \approx 0.046 e_D$ with $(-1, \sqrt{\nu})$ solitons that transform the particle system to the rotated and deformed hexagonal phase at small V . This orientationally locked phase then approaches the free floating hexagonal lattice as the substrate potential V vanishes. Quite unexpectedly, we have found that the optimal orientation of the $(0,1)$ domain wall does not follow a common symmetry axis of the substrate and the parent crystal, although such a special symmetry has often been considered as natural in the literature²². Furthermore, the geometrical constraints associated with the transformation between lattices are incompatible with the occurrence of just one solitonic transition involving simple line defects as it appears within the framework of the resonance approximation^{19,20}. An interesting scenario alternative to the one we have found in the present problem is a transformation involving the formation of a network of crossing solitons. If the most favorable solitons have close critical potentials and a negative intersection energy, the two smooth transitions may merge to a single first-order one. In our analysis of the square-to-hex transition in the dipolar system, we have found far separated values for the two transitions at $V_c^{(0,1)}$ and V_c^{PT} , favoring our scenario with two subsequent transitions and discouraging an alternative scenario involving a soliton network.

Besides a direct structural observation (in direct or reciprocal space) of the different phases appearing along the transformation pathway, an alternative way of observing the various transitions is via the system's dynamical response under an applied force field. Indeed, it turns out, that each of the phases reacts to a force field with its specific dynamical characteristic. The ordered lattices, square and period-doubled, are pinned to the optical lattice, one symmetrically along the x and y axes, the other asymmetrically with a reduced pinning along y , e.g., with a suppression factor $V/32\Delta \sim 1/8$ at $V = V_\square/2 = 4\Delta$. The domain-wall and soliton phases exhibit a very interesting dynamical response: the domain walls/solitons are (exponentially in $\sqrt{\alpha}/b$) weakly pinned by the lattice (unpinned within the continuum elastic description). A force (density) field \mathbf{f} acting on the particles will act with the line force $\mathbf{f} \cdot \mathbf{d}_{j,k}$ directed along z on the

defects. Their motion along z then produces a mass flow along the displacement field $\mathbf{d}_{j,k}$ which is longitudinal for a pure dilution defect and transverse for a pure shear defect (our domain walls and solitons are neither pure dilution nor pure shear); the observation of this characteristic flow allows for the identification of the two non-uniform phases. Finally, our analysis provides the starting point for further studies, including other pressures or densities and hence misfits, substrate lattices with different symmetries, alternative transformation scenarios, and effects due to quantum and thermal fluctuations.

We thank Matthias Troyer for helpful discussions and acknowledge financial support of the Fonds National Suisse through the NCCR MaNEP; one of us (SEK) thanks the Pauli Center for Theoretical Physics for its generous hospitality.

Appendix A: Ewald summation

The Ewald summation method²⁴ allows to sum up lattice energies for long-range interacting particles by splitting the interaction into two parts describing distant and nearby particles,

$$\frac{1}{R^\eta} = C_\eta \left\{ \int_0^\epsilon dt t^{\eta/2-1} e^{-tR^2} + \int_\epsilon^\infty dt t^{\eta/2-1} e^{-tR^2} \right\}, \quad (\text{A1})$$

with $\epsilon > 0$ a parameter and the constant C_η is given by $C_\eta^{-1} = \Gamma(\eta/2)$ with the Gamma function $\Gamma(x) = \int_0^\infty du u^{x-1} e^{-u}$. We make use of Poisson's summation formula (the set $\{K_j\}$ denote the reciprocal lattice sites, $\Omega = 1/n$ denotes the unit cell area)

$$\sum_i f(\mathbf{R}_i) = \frac{1}{\Omega} \sum_j \hat{f}(\mathbf{K}_j), \quad (\text{A2})$$

with the Fourier transform

$$\hat{f}(\mathbf{K}) = \int d^2 R f(\mathbf{R}) \exp(-i\mathbf{R} \cdot \mathbf{K}), \quad (\text{A3})$$

and treat the first (long distance) term in (A1) in Fourier space. Using the Fourier transform $\hat{f}(\mathbf{K}_j) = (\pi/t) \exp(-K_j^2/4t)$, the interaction energy per particle assumes the form

$$\begin{aligned} \frac{2e^{\text{int}}}{DC_\eta} &= \sum_{j \neq 0} \int_\epsilon^\infty dt t^{\eta/2-1} e^{-tR_j^2} \\ &\quad + \frac{\pi}{\Omega} \sum_j \int_0^\epsilon dt t^{\eta/2-2} e^{-K_j^2/4t} - \frac{2}{\eta} \epsilon^{\eta/2} \\ &= \left\{ \epsilon^{\eta/2} \left[\sum_{j \neq 0} \Psi_{\frac{\eta-2}{2}}(\epsilon R_j^2) - \frac{2}{\eta} \right] \right. \\ &\quad \left. + \frac{\pi}{\Omega} \epsilon^{\eta/2-1} \left[\frac{2}{\eta-2} + \sum_{j \neq 0} \Psi_{-\frac{\eta}{2}}(K_j^2/4\epsilon) \right] \right\}. \end{aligned} \quad (\text{A4})$$

Note that the $j = 0$ term has to be separately handled (as it is not present in the energy but contributes to the

Poisson formula) and we have substituted $t = \epsilon u$ and $t = \epsilon/u$ in the integrals of the first and second sum, respectively. The function $\Psi_x(\beta)$ is related to the Incomplete Gamma function $\Gamma(x, \beta) = \int_\beta^\infty du u^{x-1} e^{-u}$ via $\Psi_x(\beta) = \beta^{-(x+1)} \Gamma(x+1, \beta)$.

The choice $\epsilon = \pi/\Omega$ simplifies the formula (A4) substantially, as for any integers p and q the real- and K -space lattice vectors $\mathbf{R}_{p,q} = p\mathbf{R}_1 + q\mathbf{R}_2$ and $\mathbf{K}_{p,q} = p\mathbf{K}_1 + q\mathbf{K}_2 = (2\pi/\Omega)[(pR_{2y} - qR_{1y}), (-pR_{2x} + qR_{1x})]$ [note that $\mathbf{K}_1 = (2\pi/\Omega)(\mathbf{R}_2 \times \mathbf{R}_3)$, and cyclic with $\mathbf{R}_3 = (0, 0, 1)$] are related through

$$K_{p,q}^2 = (2\pi/\Omega)^2 R_{-q,p}^2. \quad (\text{A5})$$

We thus can reexpress the sum in (A4) over the reciprocal space as a sum over real space and find ($C_3 = 2/\sqrt{\pi}$)

$$e^{\text{int}} = C_\eta \pi^{\eta/2} D \Omega^{-\eta/2} \left\{ \frac{2}{\eta(\eta-2)} + \frac{1}{2} \sum_{(p,q) \neq 0} \left[\Psi_{\frac{\eta-2}{2}}(\pi R_{pq}^2/\Omega) + \Psi_{-\frac{\eta}{2}}(\pi R_{-q,p}^2/\Omega) \right] \right\}, \quad (\text{A6})$$

where the specific lattice type enters via the parameterization of the primitive lattice vectors \mathbf{R}_1 and \mathbf{R}_2 . The functions $\Psi_x(\beta)$ die off exponentially with β and the first few shells of lattice sites already give a significant contribution to the total sum, allowing for a very fast determination of the interaction energy for particles on a lattice. For any exponent $\eta > 1$ the expression (A6) assumes its global minimum for the hexagonal lattice.

Appendix B: Effective double-periodic potential

For the derivation of the effective second-mode substrate potential (27) we divide the particle lattice into two sublattices, each forming a rectangular Bravais lattice spanned by the vectors $\mathbf{a}_1 = (2b, 0)$ and $\mathbf{a}_2 = (0, b)$ and shifted with respect to one another by the vector $\mathbf{c} = (b, \delta)$. With \mathbf{R}_j^{R} denoting the sites of the rectangular lattice, the interaction energy per particle can be written as

$$e_{\text{pd}}^{\text{int}}(\delta) = \frac{1}{2} \sum_{j=1}^{N/2} \frac{D}{(R_j^{\text{R}})^3} + \frac{1}{2} \sum_{j=1}^{N/2} \frac{D}{|\mathbf{R}_j^{\text{R}} + \mathbf{c}|^3} \quad (\text{B1})$$

$$= e_{\text{R}}^{\text{int}} + \sum_{m>0} \sum_l \frac{D}{[(2m-1)^2 b^2 + (lb + \delta)^2]^{3/2}},$$

where m runs over columns, l over rows, and $e_{\text{R}}^{\text{int}} = 2.025 e_D$ is the interaction energy per particle of the rectangular lattice (given by the first sum in the first line and obtained using Ewald summation). Making use of the Poisson summation formula (A2) (with the Fourier transform (A3) and the inverse $f(\mathbf{R}) = \int [d^2 K / (2\pi)^2] \hat{f}(\mathbf{K}) \exp(i\mathbf{K} \cdot \mathbf{R})$), the sum over l takes the

form

$$\begin{aligned} & \sum_l \frac{D}{[(2m-1)^2 b^2 + (lb + \delta)^2]^{3/2}} \\ &= \sum_{l'} \int \frac{dy}{b} \frac{D e^{-2\pi i l' y/b}}{[(2m-1)^2 b^2 + (y + \delta)^2]^{3/2}} \\ &= \int \frac{dy'}{b} \frac{D}{[(2m-1)^2 b^2 + y'^2]^{3/2}} \\ & \quad + \sum_{l'>0} \int \frac{dy'}{b} \frac{D (e^{-2\pi i l' (y' - \delta)/b} + e^{2\pi i l' (y' - \delta)/b})}{[(2m-1)^2 b^2 + y'^2]^{3/2}} \\ &= \frac{2D}{(2m-1)^2 b^3} \quad (\text{B2}) \\ & \quad + \frac{8\pi D}{(2m-1)b^3} \sum_{l'>0} l' \cos(2\pi l' \delta/b) K_1[2\pi l' (2m-1)], \end{aligned}$$

with K_1 the modified Bessel function of the second kind (see Ref. 32). Inserting (B2) into (B1), the first term in Eq. (B2), corresponding to $l' = 0$, yields $2e_D \sum_{m=1}^{\infty} (2m-1)^{-2} = \pi^2 e_D/4$ and the interaction energy (B1) reads

$$e^{\text{int}}(\delta) = e_{\text{R}}^{\text{int}} + \frac{\pi^2}{4} e_D \quad (\text{B3})$$

$$+ 8\pi e_D \sum_{m>0} \sum_{l'>0} \frac{l' K_1[2\pi l' (2m-1)]}{2m-1} \cos(ql' \delta).$$

Due to the exponential decay of $K_1(z) \propto e^{-z}$, we neglect terms with $m > 1$ and $l' > 1$ in the second line and arrive at the approximative formula (19) for the interaction energy in the period-doubled phase.

Appendix C: Elastic constants

Usual pair potentials $\Phi(\mathbf{R})$ in solids involve both repulsive and attractive components at small and large distances, respectively. Such two-body potentials exhibit a minimum at a distance R_0 defining the approximate location of the equilibrium particle spacing and stabilizing the system at a specific equilibrium density. A deformation of the bulk material away from its equilibrium state contributes the elastic energy which in the continuum limit takes the form,

$$E^{\text{el}} = \frac{1}{2} \int d^d r \lambda_{\mu\nu\sigma\rho} u_{\mu\nu} u_{\sigma\rho}, \quad (\text{C1})$$

where the linearized strain tensor $u_{\mu\nu}$ and the elastic moduli $\lambda_{\mu\nu\sigma\rho}$ are given by (see standard solid state physics text books, e.g., Ref. 41)

$$u_{\mu\nu} = (\partial_\mu u_\nu + \partial_\nu u_\mu)/2, \quad (\text{C2})$$

$$\lambda_{\mu\nu\sigma\rho} = \frac{1}{8\Omega} \sum_i \{ \Phi_{\mu\sigma}(R_i) R_{i\nu} R_{i\rho} + \Phi_{\nu\sigma}(R_i) R_{i\mu} R_{i\rho} + \Phi_{\mu\rho}(R_i) R_{i\nu} R_{i\sigma} + \Phi_{\nu\rho}(R_i) R_{i\mu} R_{i\sigma} \}, \quad (\text{C3})$$

with the derivatives $\Phi_{\mu\nu} = \partial_\mu \partial_\nu \Phi$ and the unit cell area $\Omega = A/N$. These expressions implicitly assume that the system is situated in a homogeneous and isotropic ‘background’ such that rigid rotations do not cost any energy. Consequently, only the symmetric part $u_{\mu\nu}$ of the derivatives $\partial_\mu u_\nu$ enter in the formula (C3). Another problem of direct relevance in the present context is the purely repulsive two-body potential $\Phi(\mathbf{R}_{ij}) = \Phi(R_{ij})$ requiring an additional external stabilization, e.g., by adding a pressure term pA ; otherwise the repulsive particles would move apart and attain a state of vanishing density. In this situation, one should minimize the Gibbs free energy density g rather than the internal energy e . The continuum limit of the elastic energy density then reads

$$g^{\text{el}} = e^{\text{el}} + p \frac{\delta A}{A} = (\gamma_x + p)(\partial_x u_x) + (\gamma_y + p)(\partial_y u_y) \quad (\text{C4})$$

$$+ \frac{\lambda_1}{2} (\partial_x u_x)^2 + \frac{\lambda_2}{2} (\partial_y u_y)^2 + (\lambda_3 + p)(\partial_x u_x)(\partial_y u_y)$$

$$+ \frac{\lambda_4}{2} (\partial_y u_x)^2 + \frac{\lambda_5}{2} (\partial_x u_y)^2 + (\lambda_6 - p)(\partial_y u_x)(\partial_x u_y),$$

with

$$\gamma_x = \frac{1}{2\Omega} \sum_{j \neq 0} \Phi'_j \frac{x_j^2}{R_j}, \quad \gamma_y = \frac{1}{2\Omega} \sum_{j \neq 0} \Phi'_j \frac{y_j^2}{R_j}, \quad (\text{C5})$$

$$\lambda_1 = \frac{1}{2\Omega} \sum_{j \neq 0} \left[\Phi''_j - \frac{1}{R_j} \Phi'_j \right] \frac{x_j^4}{R_j^2} + \gamma_x, \quad (\text{C6})$$

$$\lambda_2 = \frac{1}{2\Omega} \sum_{j \neq 0} \left[\Phi''_j - \frac{1}{R_j} \Phi'_j \right] \frac{y_j^4}{R_j^2} + \gamma_y, \quad (\text{C7})$$

$$\lambda_3 = \frac{1}{2\Omega} \sum_{j \neq 0} \left[\Phi''_j - \frac{1}{R_j} \Phi'_j \right] \frac{x_j^2 y_j^2}{R_j^2}, \quad (\text{C8})$$

$$\lambda_4 = \frac{1}{2\Omega} \sum_{j \neq 0} \left[\Phi''_j - \frac{1}{R_j} \Phi'_j \right] \frac{x_j^2 y_j^2}{R_j^2} + \gamma_y, \quad (\text{C9})$$

$$\lambda_5 = \frac{1}{2\Omega} \sum_{j \neq 0} \left[\Phi''_j - \frac{1}{R_j} \Phi'_j \right] \frac{x_j^2 y_j^2}{R_j^2} + \gamma_x, \quad (\text{C10})$$

$$\lambda_6 = \frac{1}{2\Omega} \sum_{j \neq 0} \left[\Phi''_j - \frac{1}{R_j} \Phi'_j \right] \frac{x_j^2 y_j^2}{R_j^2}, \quad (\text{C11})$$

where we have used the abbreviations $\Phi_j \equiv \Phi(R_j)$, $\Phi'_j = d\Phi(R_j)/dR_j$, and $\Phi''_j = d^2\Phi(R_j)/dR_j^2$. Note that in Eq. (C4) we have assumed that the lattice possesses mirror symmetry along both the x - and the y -axis. Otherwise, the expression would also depend on the linear terms $(\partial_y u_x)$ and $(\partial_x u_y)$ and on the quadratic terms $(\partial_x u_x)(\partial_y u_x)$, $(\partial_x u_x)(\partial_x u_y)$, $(\partial_y u_y)(\partial_y u_x)$, and $(\partial_y u_y)(\partial_x u_y)$.

For an isotropic repulsion, the energetically most favorable configuration is a hexagonal lattice; the linear terms in Eq. (C4) have to vanish and hence $\gamma_x = \gamma_y = -p$. The pressure then is balanced by the repulsive forces via (we

use $p = -(\gamma_x + \gamma_y)/2$)

$$p = -\frac{1}{4\Omega} \sum_{j \neq 0} \Phi'(R_j) R_j = \frac{\eta}{2\Omega} e_\Delta, \quad (\text{C12})$$

where we have used that $e_\Delta = (1/2) \sum_j D/R_j^\eta$. As the right hand side of Eq. (C12) is a function of the unit cell area Ω , we obtain a relation between the applied pressure p and the area Ω or the density $n = 1/\Omega$; for $\eta = 3$, $p = 6.670 e_D n$, in agreement with Eq. (5).

1. Hexagonal Lattice

Due to the high symmetry of the hexagonal lattice, see the relations (C16), the continuum elastic energy density of Eq. (C4) simplifies to the standard form describing a homogeneous and isotropic system⁴²

$$g_\Delta^{\text{el}} = \frac{\kappa}{2} (\partial_x u_x + \partial_y u_y)^2 + \frac{\mu}{2} [(\partial_x u_x - \partial_y u_y)^2 + (\partial_y u_x + \partial_x u_y)^2], \quad (\text{C13})$$

where the shear and compression moduli μ and κ are linear combinations of the λ_j 's,

$$\kappa = \frac{\lambda_1 + \lambda_3 + p}{2}, \quad \lambda_1 = \lambda_2, \quad (\text{C14})$$

$$\mu = \frac{\lambda_1 - \lambda_3 - p}{2} = \lambda_4 = \lambda_5 = \lambda_6 - p. \quad (\text{C15})$$

The evaluation of the infinite sums is simplified considerably by first adding terms over sites \mathbf{R}_i arranged in shells of radius R_i ,

$$x_j^2 = \frac{1}{6} \sum_{s=0}^5 R_j^2 \cos^2(\vartheta_j + \frac{\pi}{3}s) = \frac{R_j^2}{2} = y_j^2,$$

$$x_j^2 y_j^2 = \frac{1}{6} \sum_{s=0}^5 R_j^4 \cos^2(\vartheta_j + \frac{\pi}{3}s) \sin^2(\vartheta_j + \frac{\pi}{3}s) = \frac{R_j^4}{8},$$

$$x_j^4 = \frac{1}{6} \sum_{s=0}^5 R_j^4 \cos^4(\vartheta_j + \frac{\pi}{3}s) = \frac{3}{8} R_j^4 = y_j^4, \quad (\text{C16})$$

where the dependence on the angle ϑ_j (with $\mathbf{R}_j = R_j \exp i\vartheta_j$) drops out due to averaging. Using these angular averages in the expressions for the elastic coefficients (C6) to (C11) and combining these with the pressure in (C12) to the elastic moduli κ and μ as given by Eqs. (C14) and (C15), we obtain the intermediate results

$$\kappa = \frac{1}{8\Omega} \sum_{j \neq 0} [\Phi''_j R_j^2 - \Phi'_j R_j], \quad (\text{C17})$$

$$\mu = \frac{1}{16\Omega} \sum_{j \neq 0} [\Phi''_j R_j^2 + 3\Phi'_j R_j].$$

Assuming an interaction potential of the form $\Phi(R) = D/R^\eta$ with $\eta > 2$, these moduli can be expressed in

terms of the interaction energy $e_\Delta = (1/2)\sum_{j\neq 0}\Phi_j$ of the hexagonal lattice and we arrive at the final results

$$\kappa = \frac{\eta(\eta+2)}{4}e_\Delta n \quad \text{and} \quad \mu = \frac{\eta(\eta-2)}{8}e_\Delta n. \quad (\text{C18})$$

The expressions (C18) scale with $n^{(\eta+2)/2}$ in particle density n ; their ratio is only determined by the exponent η of the power-law interaction potential,

$$\frac{\kappa}{\mu} = \frac{2(\eta+2)}{\eta-2}, \quad (\text{C19})$$

leading to a Poisson ratio

$$\nu = \frac{\kappa + \mu}{\kappa - \mu} = \frac{\eta + 6}{3\eta + 2}. \quad (\text{C20})$$

In our particular case with $\eta = 3$, we have $\kappa = 16.674e_D n$, $\mu = 1.667e_D n$, $\kappa = 10\mu$ and $\nu = 9/11$.

The analysis of long-range interactions with $\eta \leq 2$ requires a more careful study. For $\eta = 2$ the sum e_Δ diverges and the compression modulus becomes dispersive with $\kappa(K \rightarrow 0) \sim e_D n \ln(Kb)$, where $e_D = D/b^\eta$ is the interaction energy scale. On the other hand, for the shear modulus, the divergence of e_Δ is compensated by the factor $\eta - 2$, producing a finite result $\mu \sim e_D n$ when $\eta = 2$. Similar results have been obtained for the Wigner crystal²⁵ with $\eta = 1$ or a 2D superfluid vortex lattice with $\eta = 0$, i.e., a logarithmic interaction: the compression modulus is dispersive, $\kappa(K \rightarrow 0) \sim e_D n / (Kb)^{2-\eta}$, while the shear modulus remains finite $\mu \sim e_D n$. The calculation of the shear modulus is particularly subtle and requires an analysis with a finite screening length λ or at finite wavevector K . Interestingly, the final result turns out not to depend on λ or K and involves only short scales of order of the lattice constant.

2. Rhombic Lattices

Due to the anisotropic character of a rhombic (or isosceles triangular) lattice one finds that $\gamma_x \neq \gamma_y$ and that the linear term in the harmonic expansion Eq. (C4) does not vanish. Without further stabilization by an additional potential, an external boundary condition, etc., the system will not remain in this structure. Even though this configuration is not stable by itself in homogeneous space, it has to be invariant under global rotations. This may be checked by inserting the displacement field of a rotation by the angle φ (up to order φ^2), $u_x(\mathbf{r}) = -\varphi^2 x/2 + \varphi y$, $u_y(\mathbf{r}) = -\varphi x - s\varphi^2 y/2$ into the expression (C4). The energy change reads $\delta g^{\text{rot}} = (-\gamma_x - \gamma_y + \lambda_4 + \lambda_5 - 2\lambda_6)\varphi^2/2$ which vanishes, as easily verified using the formulas (C5) through (C11).

Applying the Ewald summation technique for $\eta = 3$ (the factors $x_j^n y_j^m$ in the expressions for the coefficients $\gamma_{x,y}$ and $\lambda_{1,\dots,6}$ are written as derivatives $\partial_{K_x j}^n \partial_{K_y j}^m \exp(-K^2/4t)$), the elastic moduli for the rhombic lattice can be combined from the expressions (the coefficients γ_y and λ_y are obtained by replacing $x^2 \rightarrow y^2$,

$K_x^2 \rightarrow K_y^2$, etc., with $y^2 = (pR_{1y} + qR_{2y})^2$ and $K_y^2 = (2\pi/\Omega)^2(-pR_{2x} + qR_{1x})^2$)

$$\gamma_x = -\frac{2\pi D}{\Omega^{5/2}} \left[1 + \frac{1}{2} \sum_{p,q} \Psi_{-\frac{3}{2}}(\pi R_{pq}^2/\Omega) \right. \quad (\text{C21})$$

$$\begin{aligned} & - \frac{\pi}{\Omega} \sum_{p,q} (pR_{2y} - qR_{1y})^2 \Psi_{-\frac{1}{2}}(\pi R_{-qp}^2/\Omega) \\ & \left. + \frac{\pi}{\Omega} \sum_{p,q} (pR_{1x} + qR_{2x})^2 \Psi_{\frac{3}{2}}(\pi R_{pq}^2/\Omega) \right], \end{aligned}$$

$$\lambda_x = \frac{1}{2\Omega} \sum_{j\neq 0} \left[\Phi_j'' - \frac{1}{R_j} \Phi_j' \right] \frac{x_j^4}{R_j^2} \quad (\text{C22})$$

$$\begin{aligned} & = \frac{4\pi D}{\Omega^{5/2}} \left[\frac{3}{2} + \frac{3}{4} \sum_{p,q} \Psi_{-\frac{3}{2}}(\pi R_{-qp}^2/\Omega) \right. \\ & + \frac{\pi^2}{\Omega^2} \sum_{p,q} (pR_{1x} + qR_{2x})^4 \Psi_{\frac{5}{2}}(\pi R_{pq}^2/\Omega) \\ & - \frac{3\pi}{\Omega} \sum_{p,q} (pR_{2y} - qR_{1y})^2 \Psi_{-\frac{1}{2}}(\pi R_{-qp}^2/\Omega) \\ & \left. + \frac{\pi^2}{\Omega^2} \sum_{p,q} (pR_{2y} - qR_{1y})^4 \Psi_{\frac{1}{2}}(\pi R_{-qp}^2/\Omega) \right], \end{aligned}$$

$$\lambda_{xy} = \frac{1}{2\Omega} \sum_{j\neq 0} \left[\Phi_j'' - \frac{1}{R_j} \Phi_j' \right] \frac{x_j^2 y_j^2}{R_j^2} \quad (\text{C23})$$

$$\begin{aligned} & = \frac{4\pi D}{\Omega^{5/2}} \left[\frac{1}{2} + \frac{1}{4} \sum_{p,q} \Psi_{-\frac{3}{2}}(\pi R_{-qp}^2/\Omega) \right. \\ & - \frac{\pi}{2\Omega} \sum_{p,q} R_{-qp}^2 \Psi_{-\frac{1}{2}}(\pi R_{-qp}^2/\Omega) \\ & + \frac{\pi^2}{\Omega^2} \sum_{p,q} (pR_{2y} - qR_{1y})^2 (-pR_{2x} + qR_{1x})^2 \Psi_{\frac{1}{2}}(\pi R_{-qp}^2/\Omega) \\ & \left. + \frac{\pi^2}{\Omega^2} \sum_{p,q} (pR_{1x} + qR_{2x})^2 (pR_{1y} + qR_{2y})^2 \Psi_{\frac{3}{2}}(\pi R_{pq}^2/\Omega) \right], \end{aligned}$$

where the terms with R_{-qp}^2 arise from the K -transformed part in the Ewald summation.

a. The bb rhombic lattice

The expansion coefficients for a rhombic lattice with height and base equal to b take the values (for convenience, we include the ‘correction’ terms $\pm p$ with $p =$

$6.670 e_D n$ with the moduli λ_3 and λ_6)

$$\gamma_x = -6.387 e_D n, \quad (\text{C24})$$

$$\gamma_y = -7.015 e_D n, \quad (\text{C25})$$

$$\kappa_x = \lambda_1 = 18.193 e_D n, \quad (\text{C26})$$

$$\kappa_y = \lambda_2 = 20.707 e_D n, \quad (\text{C27})$$

$$\kappa_{xy} = \lambda_3 + p = 14.023 e_D n, \quad (\text{C28})$$

$$\mu_x = \lambda_4 = 0.338 e_D n, \quad (\text{C29})$$

$$\mu_y = \lambda_5 = 0.967 e_D n, \quad (\text{C30})$$

$$\mu_{xy} = \lambda_6 - p = 0.684 e_D n. \quad (\text{C31})$$

b. The bb' rhombic lattice

Locking the particles to the period b along x , these form a bb' -lattice where b' adjusts itself such that the drive along y , $\gamma_y + p$ (see Eq. C4), vanishes; using the Ewald technique, we find that this is the case for $b' =$

$1.0173 b$ (alternatively, b' can be found by minimizing the Gibbs free energy $g_{b'}(b')$ at given p with respect to b' as done in Sec. V). The elastic moduli for this bb' rhombic lattice are

$$\gamma'_x = -6.155 e_D n, \quad (\text{C32})$$

$$\gamma'_y = -p = -6.670 e_D n, \quad (\text{C33})$$

$$\kappa'_x = \lambda'_1 = 17.469 e_D n, \quad (\text{C34})$$

$$\kappa'_y = \lambda'_2 = 19.531 e_D n, \quad (\text{C35})$$

$$\kappa'_{xy} = \lambda'_3 + p = 13.820 e_D n, \quad (\text{C36})$$

$$\mu'_x = \lambda'_4 = 0.480 e_D n, \quad (\text{C37})$$

$$\mu'_y = \lambda'_5 = 0.995 e_D n, \quad (\text{C38})$$

$$\mu'_{xy} = \lambda'_6 - p = 0.480 e_D n, \quad (\text{C39})$$

where we have used b as our length unit and have expressed our energy densities through $Dn^{5/2} = e_D n$.

-
- ¹ P. Bak, Reports on Progress in Physics **45**, 587 (1982).
² A.I. Larkin, Zh. Eks. Teor. Fiz. **58**, 1466 (1970) [Sov. Phys. JETP **31**, 784 (1970)].
³ E.D. Specht, M. Sutton, R.J. Birgeneau, D.E. Moncton, and P.M. Horn, Phys. Rev. B **30**, 1589 (1984); R.J. Birgeneau and P.M. Horn, Science **232**, 329 (1986).
⁴ O. Daldini, P. Martinoli, J.L. Olsen, and G. Berner, Phys. Rev. Lett. **32**, 218 (1974); A.T. Fiory, A.F. Hebard, and S. Somekh, Appl. Phys. Lett. **32**, 73 (1978).
⁵ K. Harada, O. Kamimura, H. Kasai, T. Matsuda, A. Tonomura, and V.V. Moshchalkov, Science **274**, 1167 (1996).
⁶ R.A. Webb, R.F. Voss, G. Grinstein, and P.M. Horn, Phys. Rev. Lett. **51**, 690 (1983); Ch. Leemann, Ph. Lerch, G.A. Racine, and P. Martinoli, Phys. Rev. Lett. **56**, 1291 (1986).
⁷ K. Mangold, P. Leiderer, and C. Bechinger, Phys. Rev. Lett. **90**, 158302 (2003).
⁸ J.W. Reijnders and R.A. Duine, Phys. Rev. Lett. **93**, 060401 (2004).
⁹ S. Tung, V. Schweikhard, and E.A. Cornell, Phys. Rev. Lett. **97**, 240402 (2006).
¹⁰ B. Gränz, S.E. Korshunov, V.B. Geshkenbein, and G. Blatter, Phys. Rev. B **90**, 060101(R) (2014).
¹¹ J. Doyle, B. Friedrich, R.V. Krems, and F. Masnou-Seeuws, Eur. Phys. J. D **31**, 149 (2004).
¹² K.R.A. Hazzard, B. Gadway, M. Foss-Feig, Bo Yan, S.A. Moses, J.P. Covey, N.Y. Yao, M.D. Lukin, Jun Ye, D.S. Jin, and A.M. Rey, Phys. Rev. Lett. **113**, 195302 (2014).
¹³ H.P. Büchler, E. Demler, M. Lukin, A. Micheli, N. Prokof'ev, G. Pupillo, and P. Zoller, Phys. Rev. Lett. **98**, 060404 (2007).
¹⁴ C.R. Woods, L. Britnell, A. Eckmann, R.S. Ma, J.C. Lu, H.M. Guo, X. Lin, G.L. Yu, Y. Cao, R.V. Gorbachev, A.V. Kretinin, J. Park, L.A. Ponomarenko, M.I. Katsnelson, Yu.N. Gornostyrev, K. Watanabe, T. Taniguchi, C. Casiraghi, H.-J. Gao, A.K. Geim, and K.S. Novoselov, Nature Physics **10**, 451456 (2014).
¹⁵ Y.I. Frenkel and T. Kontorowa, Zh. Eksp. Teor. Fiz. **8**, 1340 (1938).
¹⁶ F.C. Frank and J.H. Van der Merwe, Proc. R. Soc. **198** 205 (1949).
¹⁷ J.P. McTague and A.D. Novaco, Phys. Rev. B **19**, 5299 (1979).
¹⁸ V.L. Pokrovsky and A.L. Talapov, Phys. Rev. Lett. **42**, 65 (1979).
¹⁹ V.L. Pokrovskii and A.L. Talapov, Sov. Phys. JETP **51**, 134 (1980) [Zh. Eksp. Teor. Fiz. **78**, 269 (1980)].
²⁰ V.L. Pokrovsky and A.L. Talapov, *Theory of incommensurate crystals* (Harwood, Chur, 1984).
²¹ V. Zhuravlev and T. Maniv, Phys. Rev. B **68**, 174507 (2003).
²² J. Villain, in *Ordering in Two Dimensions*, ed. S. Sinha (North-Holland, New York, 1980); P.M. Chaikin and T.C. Lubensky, *Principles of Condensed Matter Physics* (Cambridge University Press, Cambridge, 1995).
²³ L.A. Bol'shov, A.P. Napartovich, A.G.N. Naumovets, and A.G. Fedoras, Sov. Phys. Usp. **20**, 432 (1977) [Usp. Fiz. Nauk **122**, 125 (1977)].
²⁴ P.P. Ewald, Ann. Phys. (Leipzig) **64**, 253 (1921).
²⁵ L. Bonsall and A.A. Maradudin, Phys. Rev. B **15**, 1959 (1977).
²⁶ In two dimensions, the real- and reciprocal-space lattice vectors are related through ($\mathbf{K}_1 = (2\pi/\Omega)(\mathbf{a}_2 \times \mathbf{a}_3)$), and cyclic with $\mathbf{a}_3 = (0, 0, 1)$, Ω denotes the unit cell area)

$$\mathbf{R}_{p,q} = p\mathbf{a}_1 + q\mathbf{a}_2,$$

$$\mathbf{K}_{p,q} = p\mathbf{K}_1 + q\mathbf{K}_2,$$

$$= \frac{2\pi}{\Omega} [(pa_{2y} - qa_{1y}), (-pa_{2x} + qa_{1x})],$$

$$K_{p,q}^2 = \left(\frac{2\pi}{\Omega}\right)^2 R_{-q,p}^2.$$

²⁷ Fixing the chemical potential and minimizing the grand potential $\omega(\mu, n) = ne_{\Delta}(n) - \mu n$ instead, we find that $\mu = (5/2)e_{\Delta}$.
²⁸ W.V. Pogosov, A.L. Rakhmanov, and V.V. Moshchalkov, Phys. Rev. B **67**, 014532 (2003).

²⁹ The associated inverse Fourier transform is defined as $\hat{\Phi}_i^D(\mathbf{R}_i) = (1/N) \sum_{\mathbf{k} \in \text{BZ}} \hat{\Phi}^D(\mathbf{k}) \exp(i\mathbf{k} \cdot \mathbf{R}_i)$.

³⁰ We define the Fourier transformation via $f(\mathbf{k}) = \sum_i f(\mathbf{R}_i) \exp(-i\mathbf{R}_i \cdot \mathbf{k})$ and its inverse via $f(\mathbf{R}_i) = (1/N) \sum_{\mathbf{k} \in \text{BZ}} f(\mathbf{k}) \exp(i\mathbf{R}_i \cdot \mathbf{k})$.

³¹ With a discrete reciprocal space, the Kronecker symbol has to be understood as the characteristic function over the mode volume $(2\pi)^2/A$.

³² M. Abramowitz und I.A. Stegun, *Handbook of Mathematical Functions* (Dover, New York, 1972).

³³ The complete elliptic integrals are approximated as

$$K\left[\sqrt{\frac{2}{2+\beta}}\right] = \frac{5}{2} \log 2 - \frac{1}{2} \log \beta + \frac{\beta}{16} (2 + 5 \log 2 - \log \beta),$$

$$E\left[\sqrt{\frac{2}{2+\beta}}\right] = 1 - \frac{\beta}{8} (1 - 5 \log 2) - \frac{\beta}{8} \log \beta,$$

where terms of order $\mathcal{O}(\beta^2 \log \beta, \beta^2)$ have been ignored.

³⁴ In Ref. 19 the Poisson ratio was mistakenly evaluated to $\nu = 5/11$ producing an angle $\theta \approx 24^\circ$ (corrected in Ref. 20).

³⁵ F.D.M. Haldane and J. Villain, *J. Phys. France* **42**, 1673 (1981).

³⁶ In a harmonic approximation, the energies due to inter- and intra-cell deformations decouple, resulting in four terms $\propto (\nabla \bar{\sigma})^2, (\nabla \bar{\delta})^2, (\nabla \bar{\delta}) \bar{\delta}$, and $\bar{\delta}^2$ (we make use of the symmetry $\bar{\delta} \rightarrow -\bar{\delta}$). We assume that the $\bar{\delta}$ -deformation remains directed along the y -axis, and that spatial variations in $\bar{\delta}$ are small. The remaining terms describe the elastic energy of the long-wavelength distortion of the bb rhombic lattice as given by $g_{\bar{\delta}}^{\text{el}}(\mathbf{v})$ and the energy of the intracell distortion that is accounted for as described in Sec. III B.

³⁷ We include here a term $p\delta A/A$.

³⁸ When starting from the square lattice, a first shear displacement field $\mathbf{u} = [0, x]/2$ takes one to the bb rhombic lattice.

³⁹ We make use of a standard minimizer algorithm, specifically the FindMinimum routine in Wolfram's Mathematica.

⁴⁰ R.K. Kalia and P. Vashishta, *J. Phys. C* **14**, L643 (1981).

⁴¹ N.W. Ashcroft and N.D. Mermin, *Solid State Physics* (Harcourt, 1967).

⁴² L.D. Landau and E.M. Lifschitz, *Course of Theoretical Physics, Vol. 7, Theory of Elasticity* (Pergamon Press, New York, 1970).